

Select autophagy genes maintain quiescence of tissue-resident macrophages and increase susceptibility to *Listeria monocytogenes*

Ya-Ting Wang^{ID 1,2*}, Konstantin Zaitsev^{ID 1,3}, Qun Lu^{1,9}, Shan Li⁴, W. Timothy Schaiff^{1,10}, Ki-Wook Kim^{1,5}, Lindsay Droit¹, Craig B. Wilen^{ID 1,11}, Chandni Desai¹, Dale R. Balce^{1,10}, Robert C. Orchard^{ID 1,12}, Anthony Orvedahl⁶, Sunmin Park¹, Darren Kreamalmeyer¹, Scott A. Handley¹, John D. Pfeifer⁷, Megan T. Baldridge^{ID 8}, Maxim N. Artyomov¹, Christina L. Stallings^{ID 2*} and Herbert W. Virgin^{ID 1,10*}

Innate and adaptive immune responses that prime myeloid cells, such as macrophages, protect against pathogens^{1,2}. However, if left uncontrolled, these responses may lead to detrimental inflammation³. Macrophages, particularly those resident in tissues, must therefore remain quiescent between infections despite chronic stimulation by commensal micro-organisms. The genes required for quiescence of tissue-resident macrophages are not well understood. Autophagy, an evolutionarily conserved cellular process by which cytoplasmic contents are targeted for lysosomal digestion, has homeostatic functions including maintenance of protein and organelle integrity and regulation of metabolism⁴. Recent research has shown that degradative autophagy, as well as various combinations of autophagy genes, regulate immunity and inflammation^{5–12}. Here, we delineate a function of the autophagy proteins Beclin 1 and FIP200—but not of other essential autophagy components ATG5, ATG16L1 or ATG7—in mediating quiescence of tissue-resident macrophages by limiting the effects of systemic interferon- γ . The perturbation of quiescence in mice that lack Beclin 1 or FIP200 in myeloid cells results in spontaneous immune activation and resistance to *Listeria monocytogenes* infection. While antibiotic-treated wild-type mice display diminished macrophage responses to inflammatory stimuli, this is not observed in mice that lack Beclin 1 in myeloid cells, establishing the dominance of this gene over effects of the bacterial microbiota. Thus, select autophagy genes, but not all genes essential for degradative autophagy, have a key function in maintaining immune quiescence of tissue-resident macrophages, resulting in genetically programmed susceptibility to bacterial infection.

L. monocytogenes is a bacterial pathogen that replicates intracellularly in macrophages until interferon- γ (IFN- γ) triggers cellular activation for effective bacterial killing^{13,14}. The involvement of autophagy in this process has been largely supported by studies in cultured cells showing that autophagy markers LC3 and

GABARAPs and p62 co-localize with structures that are either induced by or contain *L. monocytogenes*^{15–17}, and by studies that noted modestly increased *L. monocytogenes* replication in mice lacking Atg5 in myeloid cells¹⁸. Moreover, *L. monocytogenes* possesses diverse strategies to avoid degradation by autophagolysosomal pathways that may circumvent the autophagy machinery to promote pathogenesis^{15,19,20}. The precise roles of autophagy in restricting *L. monocytogenes* have therefore been challenging to reconcile. We used a genetic approach in matched littermate mice to elucidate the function of autophagy genes in resistance to *L. monocytogenes* infection. We first investigated the role of Beclin 1, a central component of the phosphatidylinositol-3-kinase (PI3K) complex that initiates autophagosome formation²¹. Compared with wild-type (WT; *Becn1^{fl/fl}*) littermates, mice lacking *Becn1* expression in myeloid cells (*Becn1^{fl/fl} Lyz2-cre^{+/-}* (*Becn1^{myeΔ}*)) were resistant to *L. monocytogenes* and controlled bacterial dissemination early after infection (Fig. 1a,c). *Fip200^{myeΔ}* mice were similarly resistant to *L. monocytogenes* (Fig. 1b,c). Notably, a previous report was unable to detect a difference in survival of *Fip200^{myeΔ}* mice when infecting with a lower dose of *L. monocytogenes*, because the non-littermate WT control mice were not susceptible to that dose¹⁷. These findings are distinct from the reported functions of another autophagy protein, ATG5, in controlling *L. monocytogenes* infection^{18,22}. We confirmed these previous results—*Atg5^{myeΔ}* mice exhibited a modest increase in *L. monocytogenes* susceptibility (Fig. 1d). By contrast, mice lacking other essential autophagy genes in myeloid cells, *Atg7^{myeΔ}* and *Atg16l1^{myeΔ}*, showed WT-level susceptibility to infection and bacteria dissemination (Fig. 1e,f, Extended Data Fig. 1a). *Atg14^{myeΔ}* mice also showed WT-level susceptibility to *L. monocytogenes*-induced lethality but harboured a reduced burden of bacteria in the liver (Fig. 1g, Extended Data Fig. 1a). The autophagy genes were all effectively excised in the macrophages of these mice as measured by p62 degradation and LC3 lipidation (Extended Data Fig. 1b). These findings were particularly notable as *Atg7^{myeΔ}* and *Atg16l1^{myeΔ}* mice from the same facility are significantly more

¹Department of Pathology and Immunology, Washington University School of Medicine, St Louis, MO, USA. ²Department of Molecular Microbiology, Washington University School of Medicine, St Louis, MO, USA. ³Computer Technologies Department, ITMO University, St Petersburg, Russia.

⁴Department of Cell Biology and Physiology, Washington University School of Medicine, St Louis, MO, USA. ⁵Department of Pharmacology, University of Illinois College of Medicine, Chicago, IL, USA. ⁶Department of Pediatrics, Division of Infectious Diseases, Washington University School of Medicine, St Louis, MO, USA. ⁷Lauren V. Ackerman Laboratory of Surgical Pathology, Division of Anatomic and Molecular Pathology, Department of Pathology and Immunology, Washington University Medical Center, St Louis, MO, USA. ⁸Department of Medicine, Division of Infectious Diseases, Washington University School of Medicine, St Louis, MO, USA. ⁹Present address: Center for Life Sciences, School of Life Sciences, Yunnan University, Kunming, China.

¹⁰Present address: Vir Biotechnology, San Francisco, CA, USA. ¹¹Present address: Yale School of Medicine, New Haven, CT, USA. ¹²Present address: University of Texas Southwestern Medical Center, Dallas, TX, USA. *e-mail: wang.yating@wustl.edu; stallings@wustl.edu; svirgin@vir.bio

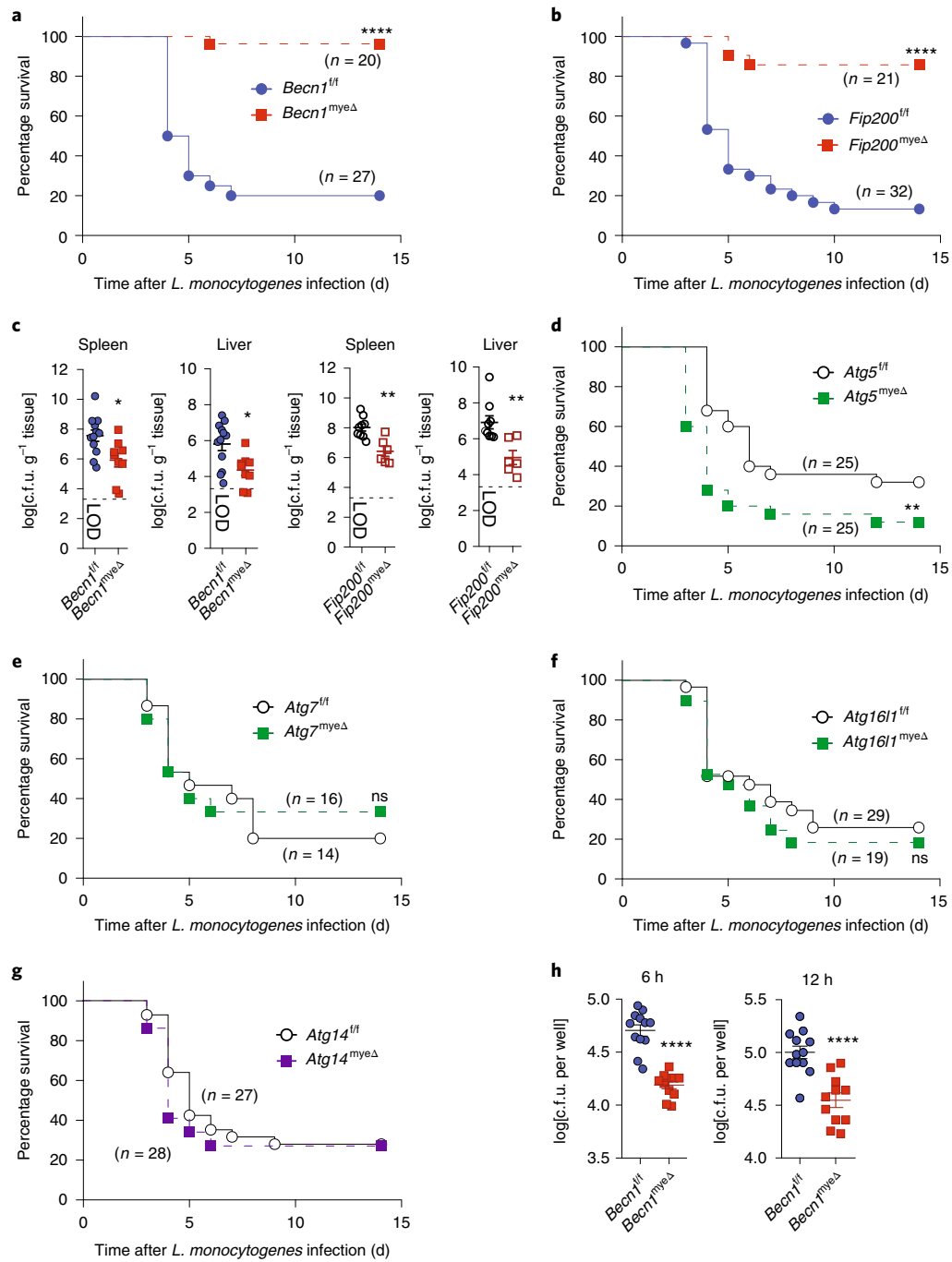


Fig. 1 | Mice with deficiencies of certain autophagy genes in myeloid cells display enhanced resistance to *L. monocytogenes*. **a,b,d–g**, Survival of mice that harbour myeloid deficiency (*myeΔ*) in autophagy genes (*Becn1* (a), *Fip200* (b), *Atg5* (d), *Atg7* (e), *Atg16l1* (f) and *Atg14* (g)) versus littermate controls, after i.p. inoculation with $4\text{--}5 \times 10^5$ colony-forming units (c.f.u.) of *L. monocytogenes*. Data were pooled from three to four experiments. *P* values were calculated using log-rank Mantel-Cox tests. Notable comparisons that were not significantly different are designated as not significant (ns). **c**, *L. monocytogenes* c.f.u. in spleen and liver 3 d after infection. Data are mean \pm s.e.m., pooled from two experiments. *Becn1^{fl/fl}*, $n=12$; *Becn1^{myeΔ}*, $n=9$; *Fip200^{fl/fl}*, $n=9$; *Fip200^{myeΔ}*, $n=6$ mice. *P* values were calculated using two-tailed t-tests. **P* < 0.05. **h**, Ex vivo bactericidal activity of purified peritoneal macrophages at the indicated times. Data are mean \pm s.e.m., pooled from two experiments. *Becn1^{fl/fl}*, $n=12$; *Becn1^{myeΔ}*, $n=11$. Adjusted *P* values were calculated using two-tailed t-tests. *****P* < 0.0001; ***P* < 0.01; **P* < 0.05.

susceptible to *T. gondii* infection, whereas *Atg5* is uniquely required to control *Mycobacterium tuberculosis*^{8,23}. Resistance to *L. monocytogenes* is therefore genetically distinct from these other infections.

Previous studies found that *L. monocytogenes* vacuolar escape and intracellular growth is independent of *Atg5* or *Becn1*^{19,24}; this led us to consider the alternative hypothesis that macrophages lacking

Beclin 1 and FIP200 are activated in vivo before infection. We therefore analysed naive macrophages that are resident in the peritoneal cavity, as these cells provide a first line of defence against intraperitoneal (i.p.) challenge with *L. monocytogenes*. Peritoneal macrophages from *Becn1^{fl/fl}* mice infected in vitro with *L. monocytogenes* showed enhanced control of the bacterial replication, demonstrating

cell-intrinsic resistance to *L. monocytogenes* (Fig. 1h, Extended Data Fig. 1c). We found that naive peritoneal resident macrophages, defined by surface markers as CSF1R⁺ICAM2⁺CD11b⁺ (ICAM2⁺ macrophages; Supplementary Fig. 1a), from *Becn1*^{myeΔ} mice showed marked upregulation of major histocompatibility complex (MHC) class II expression (Fig. 2a), whereas total peritoneal cell counts, as well as absolute numbers of ICAM2⁺ peritoneal macrophages and peripheral blood monocytes, were unaffected (Fig. 2b, Supplementary Fig. 2b). Implanted macrophages from *Becn1*^{myeΔ} mice expressed increased inducible nitric oxide synthase (iNOS) after stimulation with lipopolysaccharide (LPS) or IFN-γ (Fig. 2c), indicating that the cells were primed in vivo before infection. As *Lyz2*-cre disrupts genes in multiple cell lineages in addition to resident macrophages in the peritoneal cavity, including neutrophils, dendritic cells (DCs) and small peritoneal macrophages (SPMs)^{25,26}, we next examined the effect of Beclin 1 deletions in these other cell types. We infected *Becn1*^{fl/fl}*Mrp8*-Cre mice and *Becn1*^{fl/fl}*CD11c*-Cre mice—with deletions for *Becn1* in neutrophils and in DCs/SPMs, respectively—with *L. monocytogenes*. Loss of Beclin 1 from neutrophils or DCs and SPMs was not sufficient to result in the phenotypes observed in the *Becn1*^{myeΔ} mice (Extended Data Fig. 2), suggesting *L. monocytogenes* resistance and macrophage activation is specific to macrophage deletion of Beclin 1.

Similar to *Becn1*^{myeΔ} mice, MHC-II^{high}ICAM2⁺ macrophages were observed in naive *Fip200*^{myeΔ} mice but were absent in *Atg5*^{myeΔ}, *Atg7*^{myeΔ} and *Atg16l1*^{myeΔ} mice (Fig. 2d,e, Extended Data Fig. 3a–c). In *Atg14*^{myeΔ} mice, we observed variation in macrophage MHC-II level (Extended Data Fig. 3d). However, on average, *Atg14*^{myeΔ} mice had lower levels of MHC-II^{high}ICAM2⁺ macrophages compared with *Becn1*^{myeΔ} or *Fip200*^{myeΔ} mice (Extended Data Fig. 3e). Global knockout of *Rubicon*, a gene that mediates LC3-associated phagocytosis (LAP) and that is a repressor of degradative autophagy²⁷, had no effect on MHC-II^{high}ICAM2⁺ macrophages in naive mice (Fig. 2e, Extended Data Fig. 3b,c). Together, these data show that resistance to *L. monocytogenes* correlates with the level of MHC-II^{high}ICAM2⁺ macrophages observed in uninfected mice.

We next investigated whether the macrophage activation that occurs in the absence of Beclin 1 or FIP200 is systemic. Blood from both *Becn1*^{myeΔ} and *Fip200*^{myeΔ} mice contained increased MHC-II⁺ monocytes (Fig. 2f,g). Tissue-resident macrophages from multiple tissues of *Becn1*^{myeΔ} mice expressed higher levels of MHC-II (Fig. 2h). To determine the changes in tissue pathology that were associated with the systemic macrophage activation, we examined H&E stained sections from mice (aged 8–12 weeks) and observed mild inflammation in multiple tissues (Supplementary Fig. 2). The lungs of *Becn1*^{myeΔ} mice showed mild, patchy bronchiolitis with perivascular lymphoid aggregates without associated bronchiectasis, interstitial fibrosis, acute lung injury or vasculitis. Very mild, widely spaced periportal aggregates of chronic inflammatory cells were present in the liver of these mice, without associated fibrosis or necrosis. The kidneys showed very mild patchy interstitial chronic inflammation without associated fibrosis or vasculitis, or overt evidence of glomerulitis or glomerulosclerosis in the *Becn1*^{myeΔ} mice. The spleens of *Becn1*^{myeΔ} mice showed increased extramedullary haematopoiesis.

To better define the activation state of macrophages before infection, we performed RNA sequencing (RNA-seq) on ICAM2⁺ macrophages from the peritoneum of naive WT and *Becn1*^{myeΔ} mice. The genes of which expression was increased in the absence of Beclin 1 included interferon-stimulated genes (ISG) and inflammatory cytokines (Fig. 2i, Extended Data Fig. 4a, Supplementary Table 1). Gene set enrichment analysis demonstrated significant upregulation of IFN-γ- and IFN-αβ-responsive genes (Fig. 2j, Extended Data Fig. 4b, Supplementary Fig. 3). Quantitative PCR with reverse transcription (RT-qPCR) analysis validated findings from the RNA-seq analysis (Fig. 2k, Extended Data Fig. 4c). Upregulation of inflammatory cytokine genes *Cxcl9*, *Cxcl10* and *Ccl5* also suggested that Beclin

1-deficient macrophages were activated in naive mice (Fig. 2k). Similar upregulation of IFN response genes and inflammatory cytokines were observed in FIP200-deficient macrophages (Supplementary Fig. 4).

To understand the cellular events that are associated with pro-inflammatory macrophage activation, we analysed DNA damage responses, as accumulating evidence highlights direct links between the DNA damage response and innate immune response signalling that lead to the production of inflammatory cytokines^{28–31}. However, we did not observe changes in the DNA damage response in resting or bleomycin-treated Beclin 1-deficient macrophages compared to WT cells (Extended Data Fig. 5a). As peritoneal resident macrophages are maintained in the peritoneal cavity through self-renewal, we wondered whether macrophage activation was associated with a replication defect in Beclin 1-deficient macrophages. Peritoneal resident ICAM2⁺ macrophages from both WT and *Becn1*^{myeΔ} mice undergo slow basal in situ proliferation (Extended Data Fig. 5b). This is consistent with previous reports of low levels of BrdU⁺ proliferating macrophages in steady state²⁵.

To induce rapid local expansion of peritoneal resident macrophages, we injected mice with IL-4 complex (IL-4c)³². In WT mice, we observed increased proliferation and accumulation of ICAM2⁺ macrophages after injection with IL-4c (Extended Data Fig. 5c). By contrast, ICAM2⁺ macrophages from *Becn1*^{myeΔ} mice displayed limited replication in response to IL-4c, although they still expressed alternative activation marker RELM-α (Extended Data Fig. 5c). These results suggested that Beclin 1 regulates proliferation, but not polarization, of resident macrophages in response to IL-4c, which may be related to its function in controlling macrophage activation.

Given our observations that Beclin 1 influences activation state and proliferation of peritoneal macrophages, we performed a more global analysis of the peritoneal cell populations that rely on Beclin 1 expression in myeloid cells using single-cell transcriptomic analysis (single-cell RNA-seq). Cells from both *Becn1*^{myeΔ} and WT mice were partitioned into 20 clusters (C1–C20; Supplementary Fig. 5). Myeloid clusters (C1–C10) demonstrated a core transcriptional program of *Csf1r* (Fig. 3a,b). In WT mice, C1 and C2 represented tissue-resident peritoneal macrophages with high levels of *Adgre1*, *Timd4* and *Gata6* expression^{33–35} (Fig. 3b). We identified a macrophage subpopulation (C4) that bridges monocytes (C9) and SPMs (C8) with tissue-resident macrophages (C1 and C2; Fig. 3a). Reduced expression of genes that defined the core tissue-resident feature (*Adgre1*, *Gata6* and *Timd4*) and increased *Ccr2* levels implied that the C4 cells had a monocyte origin (Fig. 3b). This is in agreement with the idea that intermediates between newly arrived monocytes and fully mature tissue-resident macrophages are present in the peritoneum³⁶.

Cells from *Becn1*^{myeΔ} mice showed distinct clustering with the major populations shifted away from the C1 and C2 clusters present in WT mice to C3 and C4, and two distinct clusters C5 and C6 (Fig. 3a). *Becn1*^{myeΔ} ICAM2⁺ macrophages showed increased expression of IFN-pathway genes (Fig. 3c), confirming the RNA-seq analysis (Fig. 2i,j). The accumulation of intermediate C4 and the appearance of C6—macrophages with low *Adgre1*, *Gata6*, and *Timd4* expression—suggested that Beclin 1 has a function in maintaining expression of tissue-specific genes in these macrophages (Fig. 3a,b). C4 and C6 macrophages showed varying transcriptional patterns that were an intermediate between tissue-resident macrophages and monocyte-derived cells observed in WT mice (Supplementary Fig. 5d). Furthermore, compared with the WT mice, *Becn1*^{myeΔ} mice showed accumulation of *Ccr2*⁺*Itgax*[−] monocytes in C9 (Fig. 3a,b). Consistent with these findings, flow cytometry analysis identified an increase of CSF1R⁺MHC-II⁺ICAM2[−] cells in *Becn1*^{myeΔ} mice, which included an accumulation of CD226[−] monocyte-like cells and DCs, whereas the CD226⁺ SPM population was unaltered (Fig. 3d). Together these data indicate that the differentiation and activation state of resident peritoneal macrophages depends on the expression of Beclin 1.

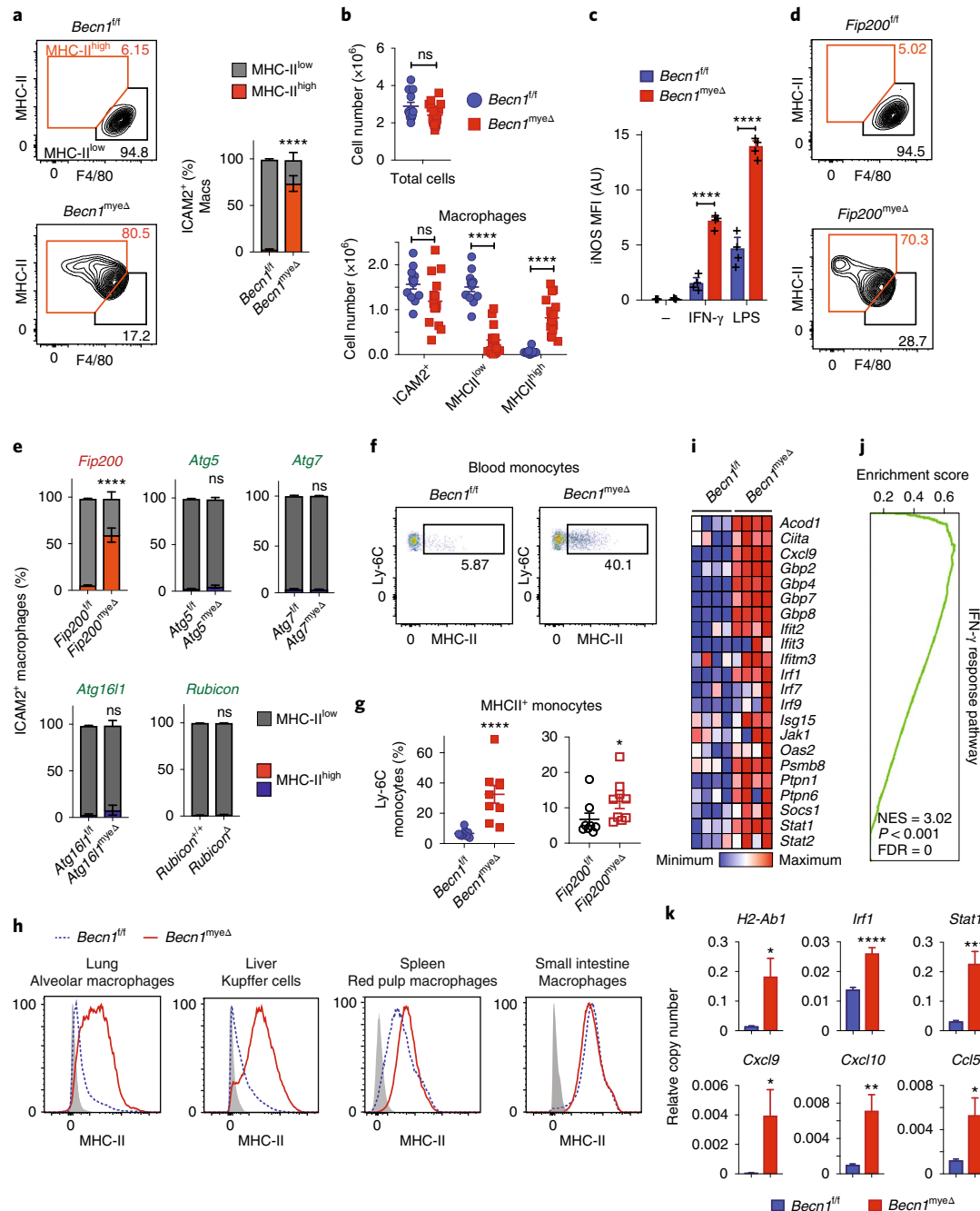


Fig. 2 | Alterations of peritoneal tissue-resident macrophages in mice with select autophagy gene deficiency. **a,d**, Flow cytometry of macrophage subsets in the peritoneum of *Becn1^{fl/fl}* and *Becn1^{mveΔ}* (**a**, left), and *Fip200^{fl/fl}* and *Fip200^{mveΔ}* (**d**) adult mice; $n \geq 3$ independent experiments with $n \geq 3$ mice. The percentage of MHC-II^{low} and MHC-II^{high} macrophages in total ICAM2⁺ macrophages (**a**, right). *Becn1^{fl/fl}*, $n=13$; *Becn1^{mveΔ}*, $n=15$. Data are mean ± s.e.m. Adjusted P values were calculated using two-way ANOVA with Sidak's multiple comparisons test on MHC-II^{high} data. **b**, The number of the total cells, and total, MHC-II^{high} and MHC-II^{low} fractions of ICAM2⁺ macrophages. Data are mean ± s.e.m., pooled from at least three experiments. *Becn1^{fl/fl}*, $n=13$; *Becn1^{mveΔ}*, $n=15$. Adjusted P values were calculated using multiple t -tests. **c**, Ex vivo stimulated peritoneal macrophages were analysed for intracellular iNOS after stimulation. Data are mean ± s.e.m., representative of three experiments; $n=4$. Adjusted P values were calculated using multiple t -tests. **e**, The percentage of MHC-II^{low} and MHC-II^{high} ICAM2⁺ macrophages; *Fip200^{fl/fl}*, $n=14$; *Fip200^{mveΔ}*, $n=15$; *Atg5^{fl/fl}*, $n=10$; *Atg5^{mveΔ}*, $n=7$; *Atg7^{fl/fl}*, $n=4$; *Atg7^{mveΔ}*, $n=4$; *Atg16l1^{fl/fl}*, $n=6$; *Atg16l1^{mveΔ}*, $n=6$; *Rubicon^{+/+}*, $n=10$; *Rubicon^{-/-}*, $n=9$ mice. Data are mean ± s.e.m. Adjusted P values were calculated using two-way ANOVA with Sidak's multiple comparisons test on MHC-II^{high} data. **f**, Flow cytometry analysis of MHC-II level on monocytes; two experiments with $n \geq 3$ biological replicates per group. **g**, The percentage of MHC-II⁺ monocytes; *Becn1^{fl/fl}*, $n=9$; *Becn1^{mveΔ}*, $n=8$; *Fip200^{fl/fl}*, $n=8$; *Fip200^{mveΔ}*, $n=8$ mice. Data are mean ± s.e.m. P values were calculated using two-tailed Mann-Whitney U -test. **h**, Flow cytometry analysis of tissue-resident macrophages; two experiments with $n \geq 3$ biological replicates per group. **i**, Heat map of selected genes regulated by Beclin 1 using RNA-seq; $n=4$ samples per group. **j**, Gene set enrichment analysis of *Becn1*-dependent signature; the green curve represents the density of the genes identified in the RNA-seq analysis with normalized enrichment score (NES). False discovery rate (FDR)-adjusted P values are indicated. **k**, RT-qPCR measurements of transcript levels in naive peritoneal macrophages. Data are mean ± s.e.m. from three independent experiments; *Becn1^{fl/fl}*, $n=9$; *Becn1^{mveΔ}*, $n=8$. P values were calculated using two-tailed Mann-Whitney U -tests. **** $P < 0.0001$; *** $P < 0.001$; ** $P < 0.01$; * $P < 0.05$.

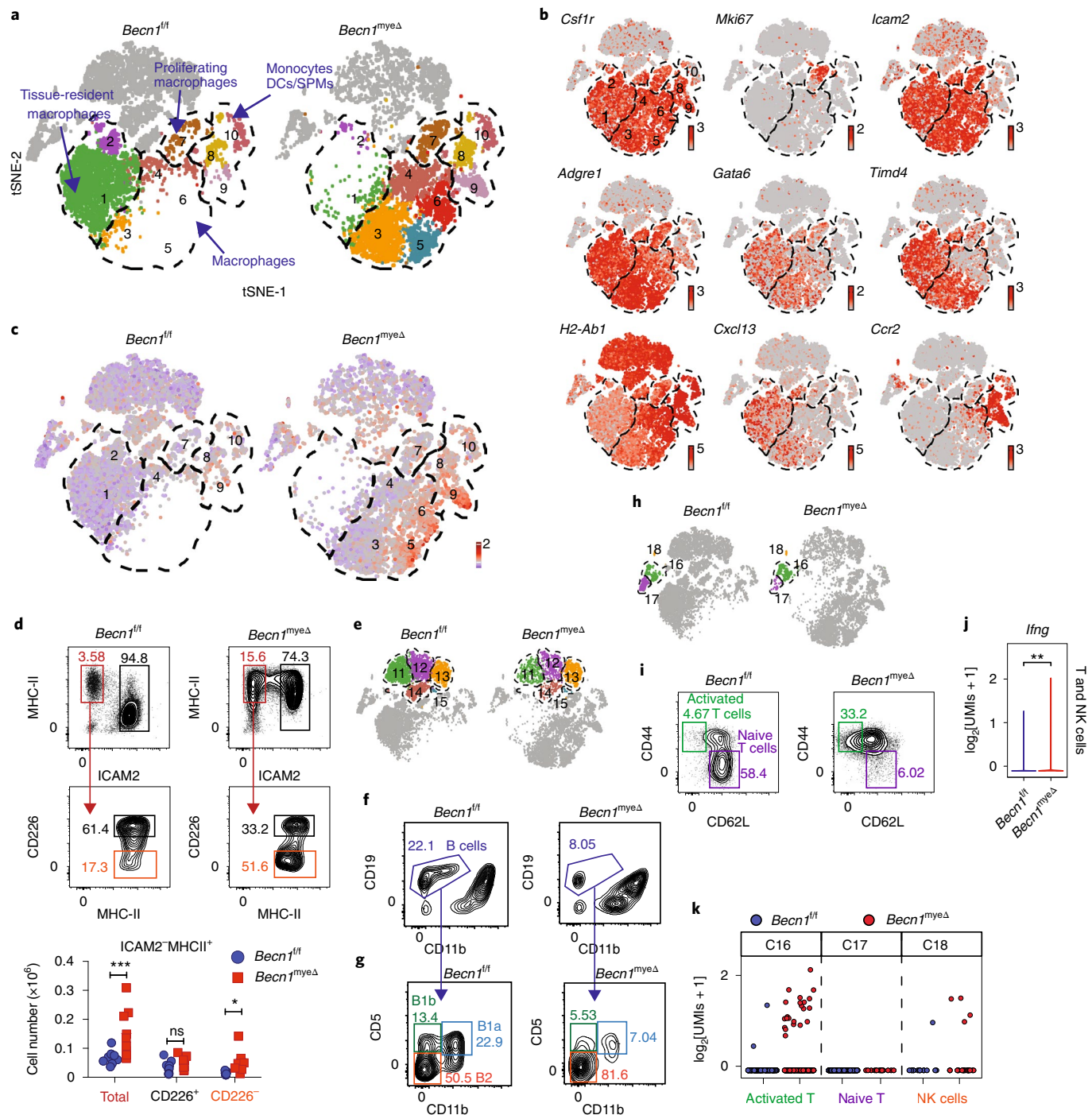


Fig. 3 | Disrupted immune cell homeostasis associated with *Beclin 1* myeloid deficiency. **a–c,e,h**, Myeloid SPMs (**a**), B-cell (**e**) and T- and NK-cell (**h**) clusters from single-cell profiles of peritoneal cavity cells visualized with *t*-distributed stochastic neighbour embedding (*t*SNE); $n=4$ naive mice, aged 8 weeks. Gene expression (**b**) and the IFN- γ pathway (**c**) was projected onto the *t*SNE plots with two groups of mice overlaid in **b**. Colour scales for each gene with the highest log-transformed expression level are shown. **d**, Flow cytometry validation on naive mice. Data are mean \pm s.e.m. from three experiments; *Beclin 1^{+/+}*, $n=8$; *Beclin 1^{myeΔ}*, $n=9$ mice. Adjusted P values were calculated using two-way ANOVA with Sidak's multiple comparisons test. **f,g,i**, Flow cytometry analysis on naive mice. Three experiments; $n \geq 3$ mice each. **j,k**, *Ifng* expression (violin plot (**j**); dot plots (**k**)) in T- and NK-cell clusters on the basis of single-cell RNA-seq analysis. Adjusted P values were calculated using model-based analysis of single-cell transcriptomics differential expression test. *** $P < 0.001$; ** $P < 0.01$; * $P < 0.05$.

We next examined the effects of myeloid cell deficiency of Beclin 1 on other peritoneal cells. B cells were grouped into *Zbtb32*⁺ B1 cells (C11, C12 and C14)³⁷, *Ccr7*⁺*Sell*⁺ B2 cells (C13) and *Mki67*⁺ proliferating B cells (C15; Fig. 3e, Extended Data Fig. 6a). Reduced B-cell numbers were observed in *Beclin 1^{myeΔ}* mice (Extended Data

Fig. 6a). Flow cytometry confirmed that total B cells and B1 cells were reduced in *Beclin 1^{myeΔ}* mice (Fig. 3f,g, Extended Data Fig. 6b), correlating with a decrease in macrophage expression of *Cxcl13* (Fig. 3b, Supplementary Fig. 5)^{35,38}. T cells were divided into naive (C16) and activated T cells (C17) on the basis of levels of *Sell*

(CD62L), *Cd44* and *Ccr7* (Fig. 3h, Extended Data Fig. 6c), with naive T cells reduced in *Becn1^{myeΔ}* mice (Fig. 3i, Extended Data Fig. 6d). Notably, *Becn1^{myeΔ}* mice showed increased *Ifng* expression in T cells and NK cells (Fig. 3j). *Ifng* transcription was mainly found in activated T cells (Fig. 3k, Extended Data Fig. 6e). These data show that deficiency of Beclin 1 in myeloid cells has considerable effects on bystander immune cells, such that immune homeostasis is substantially disrupted. Perturbed homeostasis with reduced B1 cells and activation of T cells were also observed in *Fip200^{myeΔ}* mice (Supplementary Fig. 6).

We next investigated the immune mechanism that is responsible for the disruption in the structure and function of the immune system observed in the peritoneum of *Becn1^{myeΔ}* mice. Although previous reports have linked autophagy deficiency to inflammasome activation^{6,39–41}, introduction of *Casp1/11* deficiency did not influence MHC-II levels or resistance to *L. monocytogenes* in Beclin 1-deficient macrophages (Fig. 4a,d, Extended Data Fig. 7a–c). On the basis of the increase in IFN-pathway gene expression shown in the RNA-seq and single-cell RNA-seq results, we tested the hypothesis that proinflammatory macrophage activation in uninfected mice lacking myeloid Beclin 1 is driven by IFN-γ. Although autophagy inhibits type I IFN production and the type I IFN pathway is enriched due to overlapping gene sets with IFN-γ pathway, this pathway is detrimental during *L. monocytogenes* infections^{42–45}. Introduction of IFN-γ receptor deficiency (*Ifngr^Δ*) abolished MHC-II^{high}ICAM2⁺ macrophages in *Becn1^{myeΔ}* *Ifngr^Δ* mice, indicating that IFN-γ has an essential function in the activation of macrophages in *Becn1^{myeΔ}* mice (Fig. 4a,b). *Ifngr^Δ* also restored systemic immune homeostasis, diminishing MHC-II⁺ monocyte numbers (Fig. 4c) and rescuing the abnormal phenotypes of B- and T-cell populations, monocyte accumulation and neutrophil infiltration observed in the peritoneum of *Becn1^{myeΔ}* mice (Extended Data Fig. 8).

Given the role of T-cell-derived IFN-γ in virus-induced systemic inflammation¹⁰, and the increased numbers of *Ifng⁺* T cells revealed by single-cell RNA-seq, we assessed the involvement of T cells in eliciting proinflammatory macrophages in *Becn1^{myeΔ}* mice. Elimination of T and B cells in *Rag1^Δ* mice diminished, but did not eliminate, macrophage activation (Fig. 4a,d, Extended Data Fig. 7a,b). Compared with age- and sex-matched *Becn1^{myeΔ}* mice, *Becn1^{myeΔ}* *Rag1^Δ* mice had fewer MHC-II^{high} macrophages (*Becn1^{myeΔ}* mice, 73.6% ± 8.4; *Becn1^{myeΔ}* *Rag1^Δ* mice, 27.2% ± 3.7; $P < 0.0001$). These data suggest that, although IFN-γ from T cells in the *Becn1^{myeΔ}* mice influenced macrophages, additional IFN-γ from innate immune cells can also drive macrophage activation, albeit at a lower level, in the setting of Beclin 1-deficiency. Deletion of either the IFN-γ receptor (*Becn1^{myeΔ}* *Ifngr^Δ*) or adaptive immune cells (*Becn1^{myeΔ}* *Rag1^Δ*) ablated the protective effect of *Becn1* myeloid deletion against *L. monocytogenes* (Fig. 4e,g, Extended Data Fig. 7d). Neutralizing IFN-γ also diminished the enhanced resistance to *L. monocytogenes* in *Fip200^{myeΔ}* mice (Fig. 4f). These data demonstrate that IFN-γ is required for protection against challenge with *L. monocytogenes* in *Becn1^{myeΔ}* mice and there is a critical role for activated macrophages and bystander lymphocytes in this process.

In contrast to adult mice, neonatal *Becn1^{myeΔ}* mice lacked signs of macrophage activation on around postnatal days 14–16 (Fig. 4h). The gut microbiota was previously reported to mediate ISG expression in the intestinal tissue of ATG16L1-deficient mice⁴⁶. As the acquisition and establishment of the microbiota is an important early-life event, and commensal microorganisms set the level of immune activation of immune cells in naive mice^{47–49}, we considered the possibility that the activation of tissue-resident macrophages in adult mice is influenced by the microbiota. As such, we confirmed previous studies showing that macrophages from antibiotic-treated WT mice exhibit reduced responses to IFN-γ and LPS ex vivo⁴⁷ (Fig. 4i). In contrast to WT mice, antibiotic treatment did not diminish the responsiveness of explanted macrophages from *Becn1^{myeΔ}* mice to

either IFN-γ or LPS (Fig. 4i). Consistent with these findings, antibiotic-mediated depletion of commensal bacteria had no effect on the proinflammatory activation of peritoneal resident macrophages in *Becn1^{myeΔ}* mice (Fig. 4j, Extended Data Fig. 9a). The lack of an effect of antibiotics in *Becn1^{myeΔ}* mice was not due to inefficient microbial depletion, because—as previously reported—antibiotics diminished bacterial population on the basis of quantification of 16S copies (Extended Data Fig. 9b) and reduced CD226⁺ SPMs in both *Becn1^{myeΔ}* and WT mice⁵⁰ (Fig. 4k, Extended Data Fig. 9c). Importantly, deletion of the IFN-γ receptor partially enabled the effects of the antibiotics on the activation of explanted macrophages in antibiotic-treated *Becn1^{myeΔ}* mice (Fig. 4l). This indicates that the peritoneal resident macrophages are chronically stimulated by the bacterial microbiota to maintain basal responsiveness. Beclin 1 deletion increased the activation of these cells, presenting a dominant effect over the effects of the bacterial microbiota, in a manner that requires IFN-γ. Although transient depletion of microbiota was not able to restore the quiescent macrophages in *Becn1^{myeΔ}* mice, we cannot rule out that the microbiota may play a role during the development of the activated macrophages in these mice.

Here we have demonstrated a function of Beclin 1 and FIP200 in maintaining immune quiescence of tissue-resident macrophages. Loss of *Becn1* and *Fip200* in the myeloid cells of uninfected mice perturbs the homeostasis of cell–cell communication between lymphoid and myeloid cells, prompting the production of IFN-γ by activated T cells in a feed-forward manner, leading to activation of the immune system and altered macrophage differentiation. There were considerable physiological consequences of immune quiescence regulation. Immune activation associated with myeloid deficiency in Beclin 1 or FIP200 accelerated clearance of intracellular bacteria, whereas the regulation of the basal activation state of macrophages by antibiotics was ablated. Moreover, the proliferation of peritoneal macrophages in response to IL-4 was diminished. *Becn1^{myeΔ}* mice showed increased activation of multiple tissue-resident macrophages and blood monocytes. The role of Beclin 1 in immune quiescence is therefore systemic, but the implications of this seem to be pathogen or tissue specific. For example, in contrast to our data with *L. monocytogenes*, *Becn1^{myeΔ}* mice did not exhibit enhanced resistance to pulmonary influenza infection (Extended Data Fig. 10). Resistance to influenza is observed as a result of myeloid deficiency of multiple other autophagy genes, including *Atg5* and *Atg7*, which did not increase resistance to *L. monocytogenes*⁹. Thus, in contrast to other situations in which degradative autophagy, LAP or secretion of lysosomal contents regulates aspects of immunity system^{10,11,17,51–54}, we found that Beclin 1 and FIP200 have a distinct and important function in specific aspects of immune homeostasis. This function was independent of the ubiquitin-like LC3-conjugation machinery that is required for selective autophagy and efficient generation and closure of the mammalian autophagosome⁵⁵. The role of Beclin 1 and FIP200 in maintaining immune quiescence that we observed here is therefore distinct from a previous report in which older mice (aged >52 weeks) developed lupus-like inflammatory disease owing to a deficiency in clearing dead cells that is dependent on LAP¹¹. Whereas germ-line deletion of most *Atg* genes are neonatally lethal, *Becn1^{-/-}* and *Fip200^{-/-}* homozygotes are embryonically lethal at embryonic days 7.5–15.5 (ref. ⁵⁶). This further supports the idea that Beclin 1 and FIP200 have functions outside of canonical autophagy that are critical for development or homeostasis. These differential requirements for specific autophagy genes in different cell types and in responding to different stimuli indicate that genes in this evolutionarily conserved system have multiple independent roles in inhibiting inflammation. These data further suggest that the host uses cellular stress response genes to render cells of the myeloid lineage quiescent in the basal state. The price paid for this quiescence, which probably evolved to restrict autoimmunity and to limit detrimental immune and inflammatory responses^{11,57}, is genetically programmed susceptibility to lethal bacterial infection.

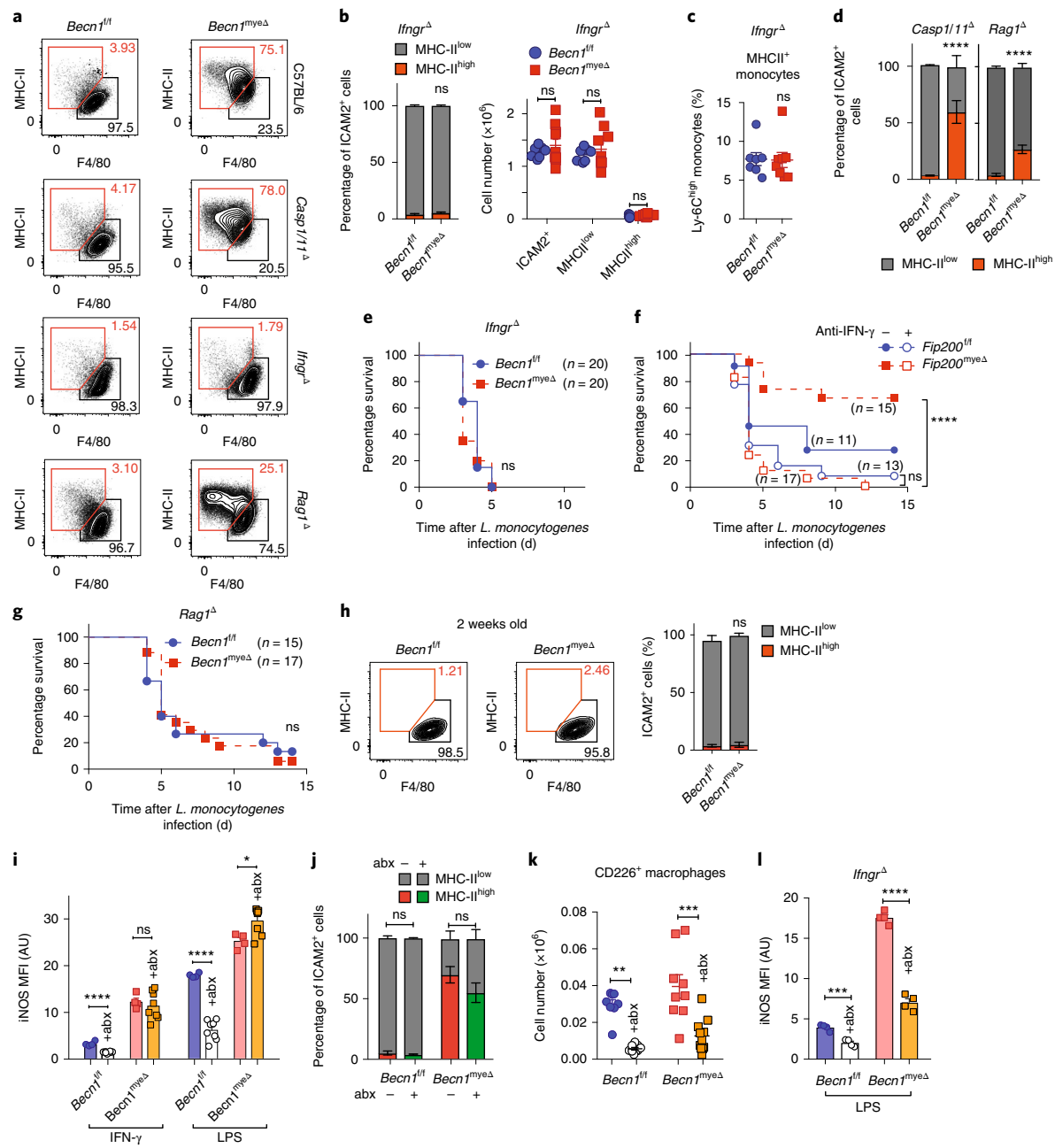


Fig. 4 | IFN- γ signalling is necessary for macrophage activation and has a dominant effect over antibiotic-mediated immune quiescence in Beclin 1 deficiency. **a**, Flow cytometry analysis of peritoneal macrophages obtained from naive adult mice. Data represent three experiments, $n \geq 3$ mice per group. **b**, Peritoneal macrophages from naive adult mice; *Becn1^{fl/fl}Ifngr^Δ*, $n=8$; *Becn1^{myleΔ}Ifngr^Δ*, $n=9$ mice. Data are mean \pm s.e.m. Statistical analysis was performed using two-way ANOVA with Sidak's multiple comparisons; no significant difference was found. **c**, The percentage of MHCII⁺ blood monocytes in naive adult mice; *Becn1^{fl/fl}Ifngr^Δ*, $n=8$; *Becn1^{myleΔ}Ifngr^Δ*, $n=9$ mice. Data are mean \pm s.e.m. Statistical analysis was performed using two-tailed Mann-Whitney U-test; no significant difference was found. **d**, The percentage of MHC-II⁺ICAM2⁺ peritoneal macrophages; *Becn1^{fl/fl}Casp11^{fl/fl}*, $n=6$; *Becn1^{myleΔ}Casp11^{fl/fl}*, $n=6$ mice. Data are mean \pm s.e.m. P values were calculated using two-way ANOVA with Sidak's multiple comparisons test. **e-g**, Survival of mice with *Ifngr^Δ* (e) and *Rag1^{fl/fl}* (g) background, and *Fip200^Δ* mice treated with antibody against IFN- γ (f) after i.p. inoculation with $4-5 \times 10^5$ c.f.u. of *L. monocytogenes*; data were pooled from three experiments. Statistical analysis was performed using log-rank Mantel-Cox tests. **h**, Flow cytometry analysis of peritoneal macrophages obtained from naive neonatal mice; *Becn1^{fl/fl}*, $n=5$; *Becn1^{myleΔ}*, $n=5$ mice. Data are mean \pm s.e.m. Statistical analysis was performed using two-way ANOVA with Sidak's multiple comparisons on MHC-II^{high} data; no significant difference was found. **i,l**, Intracellular iNOS MFI (AU) of ex vivo stimulated peritoneal macrophages from mice of C57BL/6J (i) or *Ifngr^Δ* (l) background. Three independent experiments were performed; for i, *Becn1^{fl/fl}* (Kool-Aid), $n=4$; *Becn1^{fl/fl}* (antibiotics treated (abx)), $n=8$; *Becn1^{myleΔ}* (Kool-Aid), $n=12$; *Becn1^{myleΔ}* (abx), $n=8$; for all of the groups in l, $n=4$. Data are mean \pm s.e.m. P values were calculated using two-tailed t-tests. **j**, The fractions of ICAM2⁺ macrophages. Data were pooled from at least three experiments; *Becn1^{fl/fl}* (Kool-Aid), $n=14$; *Becn1^{fl/fl}* (abx), $n=17$; *Becn1^{myleΔ}* (Kool-Aid), $n=14$; *Becn1^{myleΔ}* (abx), $n=15$. Adjusted P values were calculated using ANOVA with Tukey's multiple comparisons test on MHC-II^{high} data. **k**, Quantification of CD226⁺MHC-II⁺ICAM2⁻ SPMs. Data were pooled from at least three experiments; *Becn1^{fl/fl}* (Kool-Aid), $n=7$; *Becn1^{fl/fl}* (abx), $n=9$; *Becn1^{myleΔ}* (Kool-Aid), $n=9$; *Becn1^{myleΔ}* (abx), $n=10$; adjusted P values were calculated using two-way ANOVA with Sidak's multiple comparisons test. *** $P < 0.0001$; ** $P < 0.001$; ** $P < 0.01$; * $P < 0.05$.

Methods

Mice. *Afg5^{fl/fl}* and *Atg5^{fl/fl}-Lyz2-cre^{+/-}* mice were generated as described previously in an enhanced barrier facility^{18,58}. *Becn1^{fl/fl}-Lyz2-cre^{+/-}* (ref. ⁵⁹), *Fip200^{fl/fl}-Lyz2-cre^{+/-}* (ref. ⁶⁰), *Atg7^{fl/fl}-Lyz2-cre^{+/-}* (ref. ⁵³) and *Atg16l^{fl/fl}-Lyz2-cre^{+/-}* (ref. ⁶¹) mice were generated in the same way as the *Atg5^{fl/fl}-Lyz2-cre^{+/-}* mice. *Becn1^{fl/fl}-CD11c-cre^{+/-}* and *Becn1^{fl/fl}-Mrp8-cre^{+/-}* mice were generated by breeding *Becn1^{fl/fl}* mice with *CD11c-cre^{+/-}* (007567) and *Mrp8-cre^{+/-}* (021614) mice, respectively, from the Jackson Laboratory. *Rag1^{-/-}* (002216), *Ifngr^{-/-}* (003288) and *Casp1/11^{-/-}* (016621) mice were obtained from the Jackson Laboratory. *Rubicon^{-/-}* knockout mice were provided by D. Green and J. Martinez²⁷. All of the mice used for experimental procedures were backcrossed in-house to C57BL/6 except for *Rubicon^{-/-}* mice. Sex-matched littermates (aged 8–12 weeks) were used unless specified otherwise and were subject to randomization. Statistical consideration was not used to determine mouse sample sizes. The mice were housed and bred at Washington University in St Louis in specific pathogen-free conditions in accordance with federal and university guidelines, and protocols were approved by the Animal Studies Committee of Washington University.

L. monocytogenes and influenza virus infection. *L. monocytogenes* WT strain EGD was used for this study. *Listeria* glycerol stocks were stored at -80°C , and thawed and diluted into PBS for i.p. injection into mice. To determine tissue burden, spleens and livers were homogenized in 1 ml PBS containing 0.05% Triton X-100 and serial dilutions were plated on brain–heart infusion (BHI) agar plates. *Listeria* c.f.u. were counted after overnight growth at 37°C . The H1N1 influenza virus A strain used was A/Puerto Rico/8/1934 (PR8). Mice (aged 6–8 weeks) were infected with 250 TCID₅₀ (50% tissue culture infectious dose) of PR8 intranasally; weight loss and morbidity of the mice were monitored.

Ex vivo L. monocytogenes bactericidal essay. The protocol was adapted from previous reports⁶². In brief, peritoneal cells from naïve mice were plated in DMEM + 10% heat-inactivated fetal bovine serum (FBS) supplemented with non-essential amino acids, sodium pyruvate, HEPES, and 50 U ml⁻¹ penicillin and 50 µg ml⁻¹ streptomycin in 96-well plates (Costar) at 1×10^5 cells per well, and were allowed to adhere at 37°C . Non-adherent cells were removed by washing three times with warm antibiotic-free medium and 5×10^5 *Listeria* were put into each well. The plates were centrifuged at 600g for 5 min at room temperature to synchronize the infection of cells and were then incubated at 37°C for 15 min (time 0). After an additional 15 min at 37°C , the medium was again aspirated and changed to medium containing 5 µg ml⁻¹ gentamicin (GIBCO). At designated time points after infection, cells were washed five times in warm PBS, and were then lysed with cold sterile deionized water with 0.1% Triton X-100. Serial dilutions of lysates were plated on BHI agar plates to enumerate c.f.u.

Treatment of mice with IL-4c complexes, BrdU labelling and intracellular staining. IL-4c complexes were prepared fresh as described previously^{32,63}. IL-4 (PeproTech) and anti-IL-4 antibodies (clone, 11B11; BioXCell, BE0045) were combined at a ratio of 1:5 by mass using 1 mg ml⁻¹ cytokine and 5 mg ml⁻¹ antibody. The complexes were incubated for approximately 2 min at room temperature, diluted in PBS and injected i.p. in 300 µl volume per mouse. Control injections were 0.1% BSA diluted in 1× DPBS. Mice received injections on day 0 and day 2, followed by euthanasia on day 4. BrdU labelling was performed according to the manufacturer's protocol (BD, 552598). BrdU was injected i.p. into mice 3 h before collecting the cells. For RELM-α staining, the cells were first stained for surface markers and then permeabilized using a fixation/permeabilization solution kit (BD, 554714). After blocking with mouse and rabbit serum, the samples were stained using anti-RELM-α antibodies (PeproTech, 500-P214) for 1 h at room temperature and subsequently with secondary antibodies for 20 min at room temperature before flow cytometry analysis.

Peritoneal cell isolation, tissue leukocyte collection and flow cytometric analysis. Peritoneal cells were collected from mice after injection of 5 ml of DMEM containing 2 mM EDTA and 2% FBS into the peritoneal space. Peritoneal cells of pups were collected by 500 µl injection. Total peritoneal leukocytes were counted using an automated cell counter (Invitrogen). Blood was collected by submandibular bleeding into EDTA or lithium heparin tubes. Lungs, liver and spleen were excised, placed in DMEM containing 10% FBS, minced finely and digested at 37°C for 1 h with mechanical disruption using a stir bar and enzymatic digestion. Lung was digested with Liberase Blendzyme III (Roche), hyaluronidase (Sigma-Aldrich) and DNase I (Sigma); spleen with collagenase B (Roche) and DNase I (EMD); and liver with collagenase D and DNase I as described⁶³. Small-intestinal lamina propria cells were isolated as described previously^{9,63}. Cells were treated with ACK buffer to remove red blood cells and were passed through a 70 µm cell strainer to generate single-cell suspension.

Cells were suspended in PBS with 2 mM EDTA, 0.1% sodium azide and 3% FBS. Peritoneal cells were blocked with anti-FcγRI/III antibodies (BioLegend, 101302) and labelled with specific antibodies against CSF1R (eBioscience, 46-1152-80), ICAM2 (BioLegend, 105606), F4/80 (eBioscience, 25-4801-82), CD226 (BioLegend, 128805), Ly-6G (BioLegend, 127624), 1-A/I-E (BioLegend, 107631), CD11b (BioLegend, 101237), TCRβ (eBioscience, 11-5961-85), CD19 (BD, 552854), CD5 (BD, 553022),

CD62L (BioLegend, 104432) and CD44 (BioLegend, 103012). The total cell number was multiplied by the percentage of specific cell type in total single cells, as analysed by flow cytometry. Gating of tissue/blood cell populations was performed as described previously⁶³. In brief, blood monocytes were gated as CD45⁺Ly6C⁻CD11b. Lung alveolar macrophages were gated as CD45⁺Siglec-F⁻CD11c⁺. Liver Kupffer cells were gated as CD45⁺F4/80⁺CD11b^{low}Ly6C⁻. Spleen red pulp macrophages were gated as F4/80^{high}CD11b^{low}CD11c^{low} and negative or low for other markers. Small intestinal lamina propria macrophages were gated as CD45⁺F4/80⁺CD64⁺Ly6C⁻MHC-II⁺ (for the isotype control sample, CD45⁺F4/80⁺CD64⁺Ly6C⁻). Flow cytometric analysis was performed on an LSRLFortessa (BD Biosciences) and data were analysed using FlowJo software (Tree Star).

Peritoneal macrophage western blot, immunofluorescent and ex vivo

stimulation. Adherent macrophages were lysed using RIPA buffer (Sigma) and then diluted in 2× Laemmli buffer, resolved using 4–20% polyacrylamide gels (BioRad), transferred to PVDF membranes (BioRad) and detected using the following antibodies: anti-LC3b (Sigma, L7543), anti-p62/SQSTM1 (Sigma, P0067) and anti-GAPDH-HRP (sigma, G9295) or secondary goat-anti-Rabbit-HRP (Jackson, 111-035-144). HRP was detected using ECL (Biorad). For immunofluorescence, adherent macrophages were stimulated with 1 µg ml⁻¹ bleomycin or were not stimulated. Cells were fixed and permeabilized before staining with antibodies against γ-H2AX (clone JBW301, Millipore) and p62/SQSTM1 (GP62-C, Progen). To analyse iNOS, adherent macrophages were stimulated with 20 U ml⁻¹ recombinant IFN-γ (R&D Systems) and 10 ng ml⁻¹ LPS (Sigma). After stimulation, the medium was removed and replaced with cold PBS with 2 mM EDTA and incubated on ice for 10 min to detach the cells. The cells were first stained for live cells (Live/Dead Fixable Aqua, Invitrogen) and surface staining with antibodies. After fixation and permeabilization using BD Cytofix/Cytoperm (BD Biosciences), the cells were stained for iNOS (eBioscience 17-5920-82) and analysed using flow cytometry.

RNA Isolation, RNA-seq and RT-qPCR. For RNA-seq, peritoneal macrophages from naïve mice were purified by sorting using a Aria II flow cytometer (BD Biosciences) with >95% purity. RNA was isolated from cells using the RNeasy mini-kit (QiAGEN) and from peritoneal cells in accordance with the manufacturer's instructions. An mRNA Illumina sequencing library was generated and run on an Illumina HiSeq as previously described^{9,10}. Each group contained $n = 4$ samples, and each sample contained RNA extracted from three sorted biological replicates. DESeq2 was used for differential gene expression analysis⁶⁴, and the data from which was used as a ranked list in pre-ranked gene set enrichment analyses to identify pathway enrichment as previously described¹⁰. For RT-qPCR, RNA was extracted from sort-purified or adherent macrophages using the RNeasy mini kit (Qiagen) followed by cDNA synthesis using ImProm II (Promega). RT-qPCR using Taqman-based assays (IDT) and copy numbers were determined using a standard curve. *Actb* (IDT Assay ID: Mm.PT.58.33540333) *H2-Eb1* (IDT Assay ID: Mm.PT.58.5936748); *H2-Ab1* (IDT Assay ID: Mm.PT.58.42625719.g); *Citta* (IDT Assay ID: Mm.PT.58.41742531); *Stat1* (IDT Assay ID: Mm.PT.58.23792152); *Irf1* (IDT Assay ID: Mm.PT.58.33516776); *Cxcl9* (IDT Assay ID: Mm.PT.58.5726745); *Cxcl10* (IDT Assay ID: Mm.PT.58.43575827); *Ccl-5* (IDT Assay ID: Mm.PT.58.43548565); *Gbp4* (IDT Assay ID: Mm.PT.58.13413468); *Gbp8* (IDT Assay ID: Mm.PT.58.33178892); *Socs1* (IDT Assay ID: Mm.PT.58.11527306.g); *Igf1* (IDT Assay ID: Mm.PT.58.32726889); *Emr1* (IDT Assay ID: Mm.PT.58.11087779). Genes of interest were normalized to *Actb* copy numbers.

Single-cell RNA-seq data generation. Peritoneal cells were partitioned into nanolitre-scale Gel Bead-in-Emulsions to achieve single-cell resolution for a maximum of 10,000 individual cells per sample. Utilizing the v2 Chromium Single Cell 3' Library Kit and Chromium instrument (10x Genomics), polyadenylated mRNA from an individual cell was tagged with a unique 16 bp 10× barcode and 10 bp unique molecular identifier. Full-length cDNA was amplified to generate sufficient mass for library construction. Enzymatic fragmentation and size selection were used to optimize the cDNA amplicon size (~400 bp) for the library. The final library was sequence-ready and contained four unique sample indexes. The concentration of the 10× single cell library was determined using qPCR (Kapa Biosystems). The libraries were normalized, pooled and sequenced using a custom recipe (26–8–98) on the HiSeq4000 platform (Illumina). Two single-cell libraries were sequenced across an entire HiSeq4000 flow cell targeting approximately 90,000 reads per cell.

Alignment, barcode assignment and unique molecular identifier counting.

The Cell Ranger Single-Cell Software Suite (v.2.0.2; <https://support.10xgenomics.com/single-cell-gene-expression/software/pipelines/latest/what-is-cell-ranger>) was used to perform sample demultiplexing, barcode processing and single-cell 3' counting. Cell Ranger mkfastq was used to demultiplex raw base call files from the HiSeq4000 sequencer into sample-specific fastq files. Files were demultiplexed with 98% +perfect barcode match, and 72% +q30 reads. Subsequently, FASTQ files for each sample were processed using Cell Ranger to align reads to the mm10 genome.

Preprocessing analysis using the Seurat package. For the analysis, the Seurat package (v.2.3.4) was used⁶⁵. Genes that were filtered by barcode expression

matrices using Cell Ranger were used as analysis inputs. The samples were pooled together using the AddSample function. Expression measurements for each cell were normalized to total expression and then scaled to 10,000. Then, log normalization was performed.

Dimensionality reduction and clustering. The most variable genes were detected using FindVariableGenes function in Seurat. Principal component analysis was run using only these genes. Cells are represented with tSNE plots. We applied the RunTSNE function to normalized data, using first 10 principal components. For clustering, we used the function FindClusters, which implements a shared nearest neighbour modularity optimization-based clustering algorithm on 10 principal components with a resolution of 0.8. Twenty clusters were detected, one of which contained poorly covered cells (a lower number of unique molecular identifiers and detected genes); this cluster was excluded from further analysis.

Heat maps. All of the heat maps were generated using Phantasm web service (<https://artymovlab.wustl.edu/phantasm/>). For bulk RNA-seq, counts were log₂-quantile-normalized before heat maps were generated. For single-cell RNA-seq, scaled expression values for every gene were averaged per cluster and then log₂-normalized before heat maps were generated.

Single-cell RNA-seq differential expression. To obtain differential expression values between clusters and *Ifng* expression between conditions in T cells, a MAST test was performed and *P* values were adjusted using Bonferroni correction⁶⁶.

Antibiotic treatment of mice. Adult C57BL/6 mice were treated orally with a combination of broad-spectrum antibiotics, as previously described⁶⁷: vancomycin (0.5 g l⁻¹; Sigma-Aldrich), neomycin (1 g l⁻¹; Sigma-Aldrich), ampicillin (1 g l⁻¹; Sigma-Aldrich) and metronidazole (1 g l⁻¹; MP Biomedicals) dissolved in grape Kool-Aid (20 g l⁻¹; Kraft Foods). This solution was substituted for drinking water for 2 weeks before euthanasia and cell analysis; control mice received the grape Kool-Aid without antibiotics.

Quantification and statistical analysis. Data were analysed using Prism 7 (GraphPad Software). For all of the plots, ****P* < 0.0001, ***P* < 0.001, ***P* < 0.01, **P* < 0.05 and ns indicates not significant (*P* > 0.05) as determined by Mann–Whitney *U*-tests, Gehan–Breslow–Wilcoxon tests or two-way ANOVA with Tukey's multiple-comparison test, Kruskal–Wallis test or Sidak's multiple comparisons test, as indicated in the figure legends.

Reporting Summary. Further information on research design is available in the Nature Research Reporting Summary linked to this article.

Data availability

The data that support the findings of this study are available from the corresponding authors on reasonable request. RNA-seq data are available at the European Nucleotide Archive (PRJEB29191). Single-cell RNA-seq data are available at the GEO database (GSE121521).

Received: 23 January 2019; Accepted: 5 November 2019;

Published online: 20 January 2020

References

- Barton, E. S. et al. Herpesvirus latency confers symbiotic protection from bacterial infection. *Nature* **447**, 326–329 (2007).
- Netea, M. G. et al. Trained immunity: a program of innate immune memory in health and disease. *Science* **352**, aaf1098 (2016).
- Medzhitov, R. Origin and physiological roles of inflammation. *Nature* **454**, 428–435 (2008).
- Mizushima, N. & Komatsu, M. Autophagy: renovation of cells and tissues. *Cell* **147**, 728–741 (2011).
- Cadwell, K. et al. A key role for autophagy and the autophagy gene *Atg16l1* in mouse and human intestinal Paneth cells. *Nature* **456**, 259–263 (2008).
- Saitoh, T. et al. Loss of the autophagy protein Atg16l1 enhances endotoxin-induced IL-1 β production. *Nature* **456**, 264–268 (2008).
- Levine, B., Mizushima, N. & Virgin, H. W. Autophagy in immunity and inflammation. *Nature* **469**, 323–335 (2011).
- Kimmey, J. M. et al. Unique role for ATG5 in neutrophil-mediated immunopathology during *M. tuberculosis* infection. *Nature* **528**, 565–569 (2015).
- Lu, Q. et al. Homeostatic control of innate lung inflammation by Vici syndrome gene *Epg5* and additional autophagy genes promotes influenza pathogenesis. *Cell Host Microbe* **19**, 102–113 (2016).
- Park, S. et al. Autophagy genes enhance murine gammaherpesvirus 68 reactivation from latency by preventing virus-induced systemic inflammation. *Cell Host Microbe* **19**, 91–101 (2016).
- Martinez, J. et al. Noncanonical autophagy inhibits the autoinflammatory, lupus-like response to dying cells. *Nature* **533**, 115–119 (2016).
- Cunha, L. D. et al. LC3-associated phagocytosis in myeloid cells promotes tumor immune tolerance. *Cell* **175**, 429–441 (2018).
- Huang, S. et al. Immune response in mice that lack the interferon-gamma receptor. *Science* **259**, 1742–1745 (1993).
- Ubanue, E. R. Inter-relationship among macrophages, natural killer cells and neutrophils in early stages of *Listeria* resistance. *Curr. Opin. Immunol.* **9**, 35–43 (1997).
- Yoshikawa, Y. et al. *Listeria monocytogenes* ActA-mediated escape from autophagic recognition. *Nat. Cell Biol.* **11**, 1233–1240 (2009).
- Yano, T. et al. Autophagic control of *Listeria* through intracellular innate immune recognition in *Drosophila*. *Nat. Immunol.* **9**, 908–916 (2008).
- Gluschko, A. et al. The β 2 integrin mac-1 induces protective LC3-associated phagocytosis of *Listeria monocytogenes*. *Cell Host Microbe* **23**, 324–337 (2018).
- Zhao, Z. et al. Autophagosome-independent essential function for the autophagy protein Atg5 in cellular immunity to intracellular pathogens. *Cell Host Microbe* **4**, 458–469 (2008).
- Meyer-Morse, N. et al. Listeriolysin O is necessary and sufficient to induce autophagy during *Listeria monocytogenes* infection. *PLoS ONE* **5**, e8610 (2010).
- Huang, J. & Brumell, J. H. Bacteria-autophagy interplay: a battle for survival. *Nat. Rev. Microbiol.* **12**, 101–114 (2014).
- Liang, X. H. et al. Induction of autophagy and inhibition of tumorigenesis by beclin 1. *Nature* **402**, 672–676 (1999).
- Lee, H. K. et al. In vivo requirement for Atg5 in antigen presentation by dendritic cells. *Immunity* **32**, 227–239 (2010).
- Choi, J. et al. The parasitophorous vacuole membrane of *Toxoplasma gondii* is targeted for disruption by ubiquitin-like conjugation systems of autophagy. *Immunity* **40**, 924–935 (2014).
- Mitchell, G. et al. *Listeria monocytogenes* triggers noncanonical autophagy upon phagocytosis, but avoids subsequent growth-restricting xenophagy. *Proc. Natl Acad. Sci. USA* **115**, E210–E217 (2018).
- Cain, D. W. et al. Identification of a tissue-specific, C/EBP β -dependent pathway of differentiation for murine peritoneal macrophages. *J. Immunol.* **191**, 4665–4675 (2013).
- Galluzzi, L. et al. Autophagy in malignant transformation and cancer progression. *EMBO J.* **34**, 856–880 (2015).
- Martinez, J. et al. Molecular characterization of LC3-associated phagocytosis reveals distinct roles for Rubicon, NOX2 and autophagy proteins. *Nat. Cell Biol.* **17**, 893–906 (2015).
- Hartlava, A. et al. DNA damage primes the type I interferon system via the cytosolic DNA sensor STING to promote anti-microbial innate immunity. *Immunity* **42**, 332–343 (2015).
- Liang, Q. et al. Crosstalk between the cGAS DNA sensor and Beclin-1 autophagy protein shapes innate antimicrobial immune responses. *Cell Host Microbe* **15**, 228–238 (2014).
- Rodier, F. et al. Persistent DNA damage signalling triggers senescence-associated inflammatory cytokine secretion. *Nat. Cell Biol.* **11**, 973–979 (2009).
- West, A. P. et al. Mitochondrial DNA stress primes the antiviral innate immune response. *Nature* **520**, 553–557 (2015).
- Jenkins, S. J. et al. Local macrophage proliferation, rather than recruitment from the blood, is a signature of TH2 inflammation. *Science* **332**, 1 284–1288 (2011).
- Gautier, E. L. et al. Gata6 regulates aspartoacylase expression in resident peritoneal macrophages and controls their survival. *J. Exp. Med.* **211**, 1525–1531 (2014).
- Rosas, M. et al. The transcription factor Gata6 links tissue macrophage phenotype and proliferative renewal. *Science* **344**, 645–648 (2014).
- Okabe, Y. & Medzhitov, R. Tissue-specific signals control reversible program of localization and functional polarization of macrophages. *Cell* **157**, 832–844 (2014).
- Bain, C. C. et al. Long-lived self-renewing bone marrow-derived macrophages displace embryo-derived cells to inhabit adult serous cavities. *Nat. Commun.* **7**, ncomms11852 (2016).
- Mabbott, N. A. & Gray, D. Identification of co-expressed gene signatures in mouse B1, marginal zone and B2 B-cell populations. *Immunology* **141**, 79–95 (2014).
- Ansel, K. M., Harris, R. B. & Cyster, J. G. CXCL13 is required for B1 cell homing, natural antibody production, and body cavity immunity. *Immunity* **16**, 67–76 (2002).
- Shi, C. S. et al. Activation of autophagy by inflammatory signals limits IL-1 β production by targeting ubiquitinated inflammasomes for destruction. *Nat. Immunol.* **13**, 255–263 (2012).
- Nakahira, K. et al. Autophagy proteins regulate innate immune responses by inhibiting the release of mitochondrial DNA mediated by the NALP3 inflammasome. *Nat. Immunol.* **12**, 222–230 (2011).
- Santeford, A. et al. Impaired autophagy in macrophages promotes inflammatory eye disease. *Autophagy* **12**, 1876–1885 (2016).
- Auerbuch, V., Brockstedt, D. G., Meyer-Morse, N., O'Riordan, M. & Portnoy, D. Mice lacking the type I interferon receptor are resistant to *Listeria monocytogenes*. *J. Exp. Med.* **200**, 527–533 (2004).

43. Carrero, J. A., Calderon, B. & Unanue, E. R. Type I interferon sensitizes lymphocytes to apoptosis and reduces resistance to *Listeria* infection. *J. Exp. Med.* **200**, 535–540 (2004).
44. O'Connell, R. M. et al. Type I interferon production enhances susceptibility to *Listeria monocytogenes* infection. *J. Exp. Med.* **200**, 437–445 (2004).
45. Pitts, M. G., Myers-Morales, T., D'Orazio, S. E. & Type, I. IFN does not promote susceptibility to foodborne *Listeria monocytogenes*. *J. Immunol.* **196**, 3109–3116 (2016).
46. Martin, P. K. et al. Autophagy proteins suppress protective type I interferon signalling in response to the murine gut microbiota. *Nat. Microbiol.* **3**, 1131–1141 (2018).
47. Abt, M. C. et al. Commensal bacteria calibrate the activation threshold of innate antiviral immunity. *Immunity* **37**, 158–170 (2012).
48. Ichinohe, T. et al. Microbiota regulates immune defense against respiratory tract influenza A virus infection. *Proc. Natl Acad. Sci. USA* **108**, 5354–5359 (2011).
49. Steed, A. L. et al. The microbial metabolite desaminotyrosine protects from influenza through type I interferon. *Science* **357**, 498–502 (2017).
50. Kim, K. W. et al. MHC II⁺ resident peritoneal and pleural macrophages rely on IRF4 for development from circulating monocytes. *J. Exp. Med.* **213**, 1951–1959 (2016).
51. Kanayama, M., He, Y. W. & Shinohara, M. L. The lung is protected from spontaneous inflammation by autophagy in myeloid cells. *J. Immunol.* **194**, 5465–5471 (2015).
52. Biering, S. B. et al. Viral replication complexes are targeted by LC3-guided interferon-inducible GTPases. *Cell Host Microbe* **22**, 74–85 (2017).
53. DeSelm, C. J. et al. Autophagy proteins regulate the secretory component of osteoclastic bone resorption. *Dev. Cell* **21**, 966–974 (2011).
54. Medina, D. L. et al. Transcriptional activation of lysosomal exocytosis promotes cellular clearance. *Dev. Cell* **21**, 421–430 (2011).
55. Tsukiyama, K. et al. The ATG conjugation systems are important for degradation of the inner autophagosomal membrane. *Science* **354**, 1036–1041 (2016).
56. Kuma, A., Komatsu, M. & Mizushima, N. Autophagy-monitoring and autophagy-deficient mice. *Autophagy* **13**, 1619–1628 (2017).
57. Fernandez, A. F. et al. Disruption of the beclin 1-BCL2 autophagy regulatory complex promotes longevity in mice. *Nature* **558**, 136–140 (2018).
58. Miller, B. C. et al. The autophagy gene ATG5 plays an essential role in B lymphocyte development. *Autophagy* **4**, 309–314 (2008).
59. Sanjuan, M. A. et al. Toll-like receptor signaling in macrophages links the autophagy pathway to phagocytosis. *Nature* **450**, 1253–1257 (2007).
60. Gan, B. et al. Role of FIP200 in cardiac and liver development and its regulation of TNF α and TSC-mTOR signaling pathways. *J. Cell Biol.* **175**, 121–133 (2006).
61. Hwang, S. et al. Nondegradative role of Atg5-Atg12/ Atg16L1 autophagy protein complex in antiviral activity of interferon gamma. *Cell Host Microbe* **11**, 397–409 (2012).
62. MacDuff, D. A. et al. Phenotypic complementation of genetic immunodeficiency by chronic herpesvirus infection. *eLife* **4**, e04494 (2015).
63. Jarjour, N. N. et al. Blh40 mediates tissue-specific control of macrophage proliferation in homeostasis and type 2 immunity. *Nat. Immunol.* **20**, 687–700 (2019).
64. Love, M. I., Huber, W. & Anders, S. Moderated estimation of fold change and dispersion for RNA-seq data with DESeq2. *Genome Biol.* **15**, 550 (2014).
65. Butler, A., Hoffman, P., Smibert, P., Papalex, E. & Satija, R. Integrating single-cell transcriptomic data across different conditions, technologies, and species. *Nat. Biotechnol.* **36**, 411–420 (2018).
66. Finak, G. et al. MAST: a flexible statistical framework for assessing transcriptional changes and characterizing heterogeneity in single-cell RNA sequencing data. *Genome Biol.* **16**, 278 (2015).
67. Baldridge, M. T. et al. Commensal microbes and interferon- λ determine persistence of enteric murine norovirus infection. *Science* **347**, 266–269 (2015).

Acknowledgements

We thank G. J. Randolph, B. T. Edelson, D. Bhattacharya and the former members of the Virgin laboratory for discussion; J. R. Brestoff and S. Piersma for reading the manuscript; C. Yokoyama and H. Deng for technical assistance; and staff at the McDonnell Genome Institute, Genome Technology Access Center, Flow Cytometry Core Facility, Molecular Microbiology Imaging Facility, Pulmonary Morphology Core, and Center for Human Immunology & Immunotherapy Programs at Washington University School of Medicine for technical support. The research was supported by NIH grant U19 AI109725 and the Crohn's and Colitis Foundation grant no. 326556 (to H.W.V.), NIH grant U19 AI42784 (to H.W.V. and C.L.S) and NIH grant R01 AI132697 (to C.L.S.). Authors receive support from MES of Russia (project 2.3300.2017/4.6; to K.Z.); NIH K08 (A128043; to C.B.W.); Pediatric Infectious Diseases Society/St Jude Children's Research Hospital fellowship in basic research (to A.O.); Young Investigators Grant for Probiotics Research from the Global Probiotics Council (to M.T.B.); and Burroughs Wellcome Fund Investigators in the Pathogenesis of Infectious Disease (to C.L.S.).

Author contributions

Y.-T.W. designed the project, performed experiments, analysed the data and wrote the manuscript. H.W.V. supervised project design and edited the manuscript. C.L.S. assisted with project design and edited the manuscript. Q.L., S.L., W.T.S., L.D. and C.B.W. performed experiments. K.-W.K., D.R.B., R.C.O., A.O., S.P., D.K. and M.T.B. assisted with experiments or project design. C.D. and S.A.H. helped to design RNA-seq experiments and analyse the data. K.Z. and M.N.A. analysed RNA-seq and single-cell RNA-seq data. J.D.P. analysed the histology. All of the authors read and edited the manuscript.

Competing interests

H.W.V. is a founder of Casma Therapeutics and PierianDx. The work reported here was not funded by either company.

Additional information

Extended data is available for this paper at <https://doi.org/10.1038/s41564-019-0633-0>.

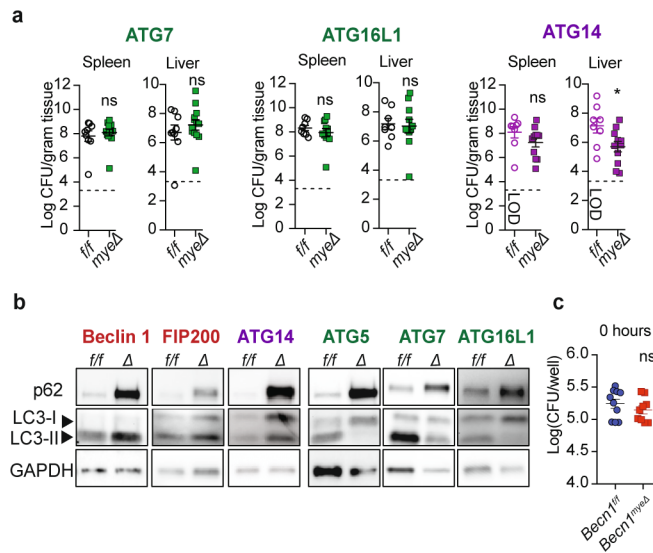
Supplementary information is available for this paper at <https://doi.org/10.1038/s41564-019-0633-0>.

Correspondence and requests for materials should be addressed to Y.-T.W., C.L.S. or H.W.V.

Reprints and permissions information is available at www.nature.com/reprints.

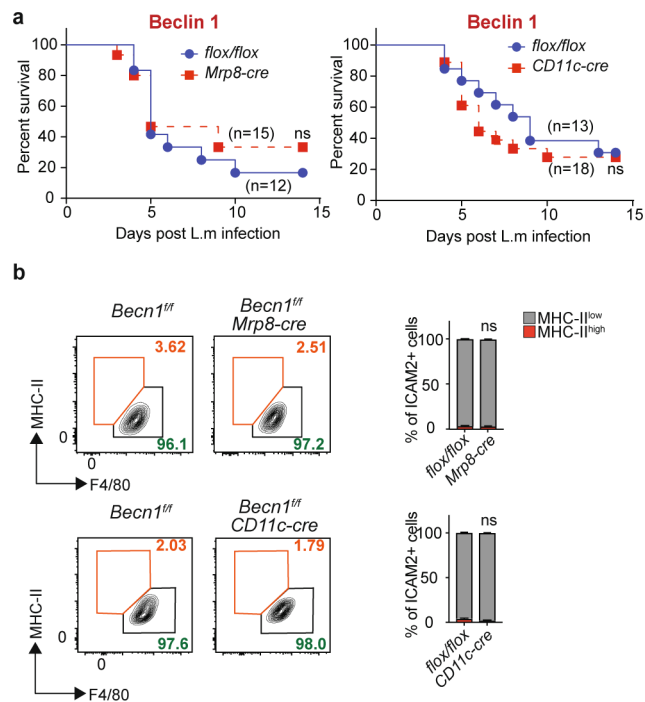
Publisher's note Springer Nature remains neutral with regard to jurisdictional claims in published maps and institutional affiliations.

© The Author(s), under exclusive licence to Springer Nature Limited 2020

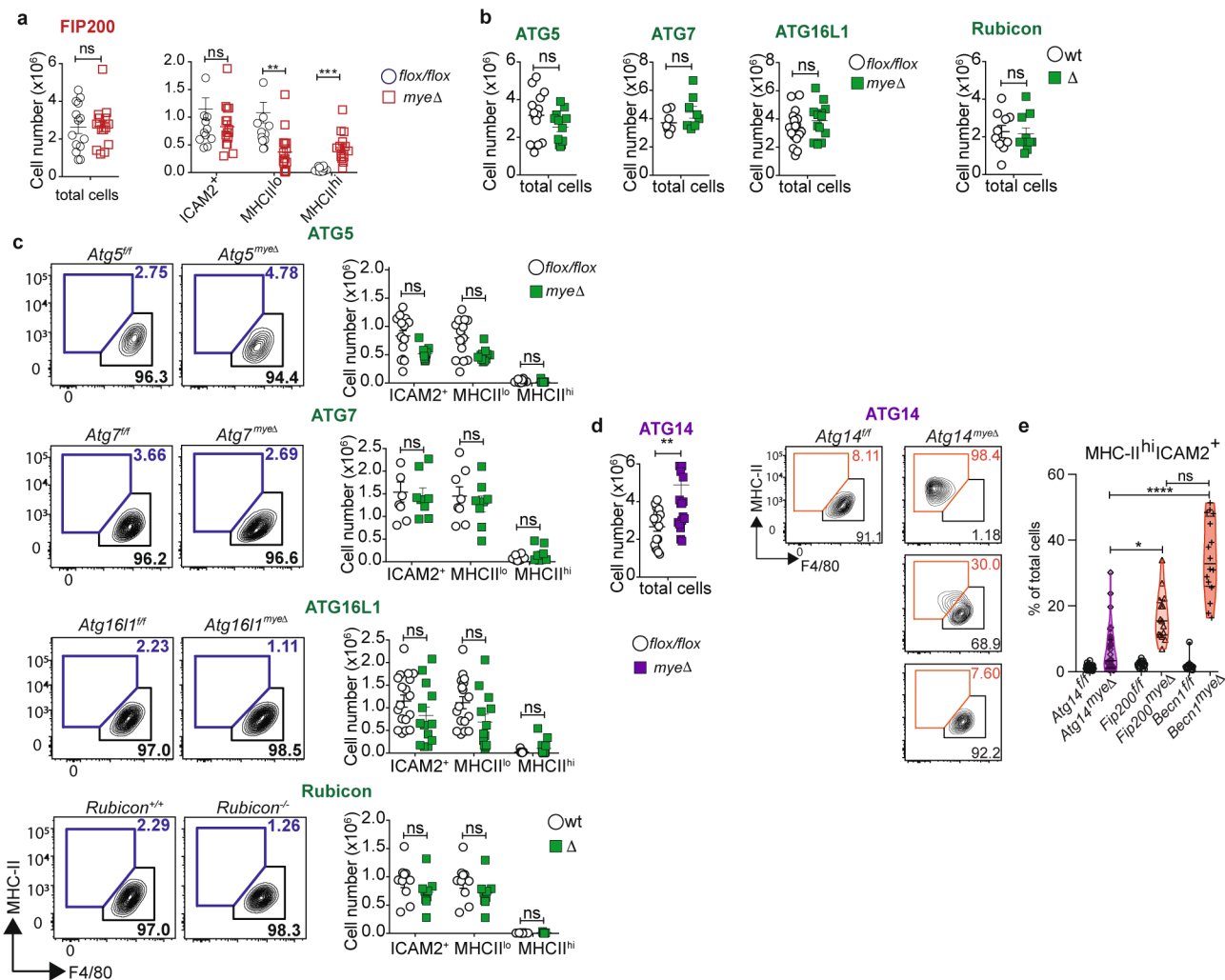

Extended Data Fig. 1 | Mice with deficiencies of certain autophagy genes in myeloid cells display enhanced resistance to *L. monocytogenes*.

a, *L. monocytogenes* CFU in spleen or liver 3 days after infection of mice harboring myeloid deficiency ($mye\Delta$) in multiple autophagy genes (data pooled from 2 experiments, $Atg7^{f/f}$, $n=9$; $Atg7^{mye\Delta}$, $n=13$; $Atg16l1^{f/f}$, $n=8$; $Atg16l1^{mye\Delta}$, $n=10$; $Atg14^{f/f}$, $n=8$; $Atg14^{mye\Delta}$, $n=11$ mice; mean \pm s.e.m.; P by 2-tailed t test).

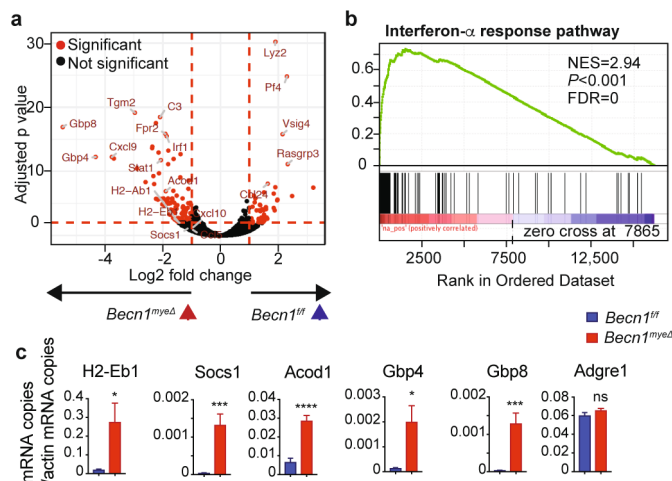
b, Western blot analysis of p62, LC3 and GAPDH in peritoneal macrophages from naïve mice (Representative of $n \geq 3$ replicates). **c**, Ex vivo phagocytosis activity of peritoneal macrophages at 0 hour (data pooled from 2 experiments, $Beclin^{f/f}$, $n=12$; $Beclin^{mye\Delta}$, $n=11$; mean \pm SEM; ns=not significant by 2-tailed t test).



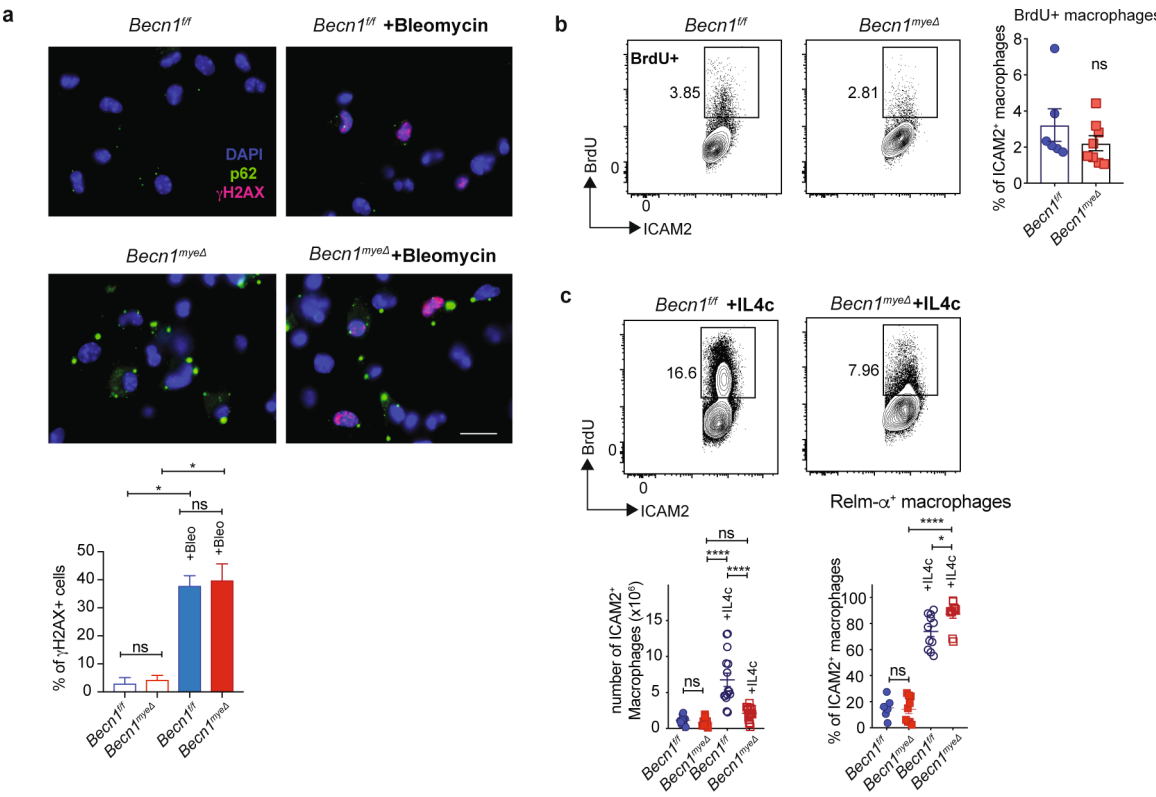
Extended Data Fig. 2 | Mice with Beclin 1 deletion in DCs or neutrophils do not display *L. monocytogenes* resistance or macrophage activation phenotype. **a**, Survival of mice harboring Beclin 1 deletion in CD11c⁺ and MRP8⁺ cells vs littermate controls, after i.p. inoculation with 4–5×10⁵ CFUs of *L. monocytogenes* (Data pooled from 3–4 experiments; not significantly different by Log-rank Mantel-Cox test). **b**, Flow cytometry of ICAM2⁺ macrophage subsets in peritoneum of adult naïve mice (Data represents 2 experiments, *Beclin 1*^{fl/fl}, n=3 vs *Beclin 1*^{fl/fl}-*Mrp8-cre*, n=3; *Beclin 1*^{fl/fl}, n=5 vs *Beclin 1*^{fl/fl}-*CD11c-cre*, n=4; mean ± SEM; not significant by 2way ANOVA Sidak's multiple comparisons).



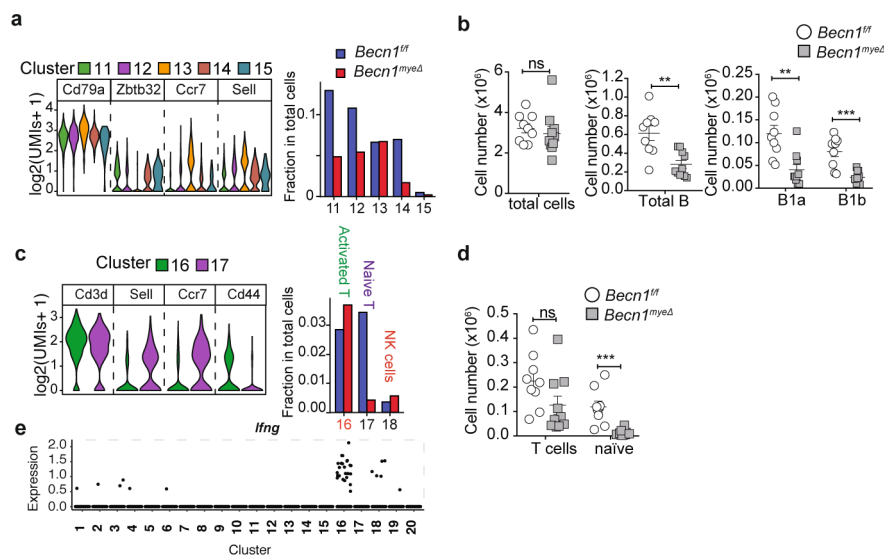
Extended Data Fig. 3 | Alterations of peritoneal tissue resident macrophages in mice with central autophagy gene deficiency. **a, b, c, d,** Quantification of number of total cells, total ICAM2⁺ macrophages, and numbers of MHC-II^{high} and MHC-II^{low} fractions of ICAM2⁺ macrophages from peritoneum lavage of mice harboring myeloid deficiency (*myeΔ*) in multiple autophagy genes and total deficiency (Δ) of Rubicon. (Data pooled from ≥ 3 independent experiments: *Fip200*^{fl/fl}, $n=14$; *Fip200*^{myeΔ}, $n=16$; *Atg5*^{fl/fl}, $n=14$; *Atg5*^{myeΔ}, $n=12$; *Atg7*^{fl/fl}, $n=8$; *Atg7*^{myeΔ}, $n=8$; *Atg16l*^{fl/fl}, $n=18$; *Atg16l*^{myeΔ}, $n=13$; *Rubicon* WT, $n=10$; *Rubicon* KO, $n=9$; *Atg14*^{fl/fl}, $n=16$; *Atg14*^{myeΔ}, $n=15$ mice; mean \pm SEM; P , or P_{adj} for multiple comparison with 2-tailed t test). **e,** Violin plot showing percent of MHC-II^{high}ICAM2⁺ macrophages in total peritoneal immune cells (*Atg14*^{fl/fl}, $n=42$; *Atg14*^{myeΔ}, $n=38$; *Becn1*^{fl/fl}, $n=12$; *Becn1*^{myeΔ}, $n=16$; *Fip200*^{fl/fl}, $n=15$; *Fip200*^{myeΔ}, $n=15$; mean \pm SEM; P_{adj} by Kruskal-Wallis Dunn's multiple comparison test).



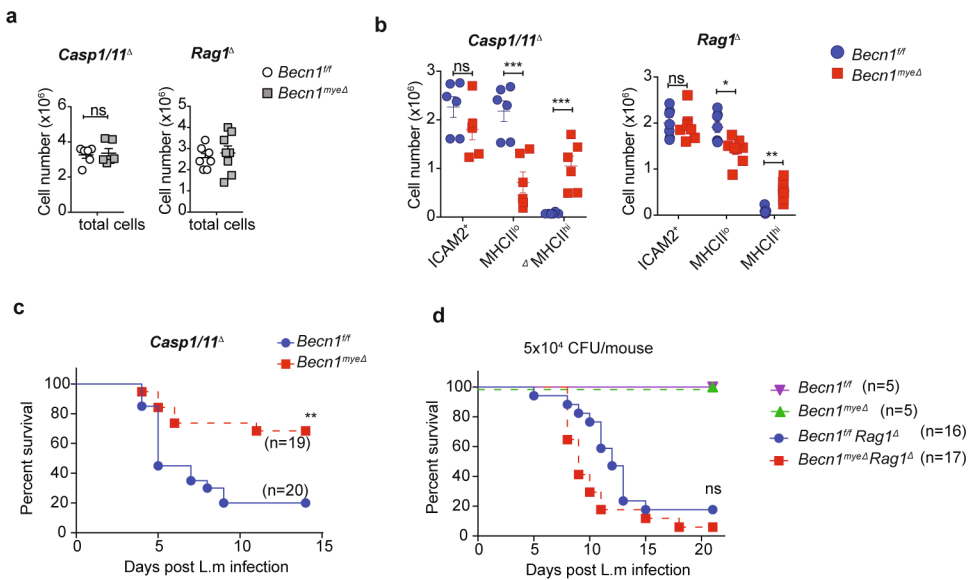
Extended Data Fig. 4 | Beclin 1 deficiency augmented baseline macrophage IFN signaling. **a**, Volcano plot shows genes upregulated in macrophages from *Beclin1^{myeΔ}* mice on the left and downregulated on the right in RNA-seq data set (*Beclin1^{ff}*, $n=4$; *Beclin1^{myeΔ}*, $n=4$). **b**, Gene set enrichment analysis of *Beclin1* dependent signature. (The green curve represents the density of the genes identified in the RNAseq with Normalized Enrichment Score (NES), P value and False Discovery Rate (FDR) listed.) **c**, Transcript levels of the indicated genes in naïve peritoneal macrophages. (3 independent experiments, *Beclin1^{ff}*, $n=9$; *Beclin1^{myeΔ}*, $n=8$; mean \pm SEM; P by 2-tailed t test.).



Extended Data Fig. 5 | DNA damage response and cell proliferation of Beclin 1 deficient peritoneal macrophages. **a**, The presence of DNA double-strand break were revealed by immunofluorescence for γ -H2AX (red) in peritoneal macrophages treated with Bleomycin for 6 hours or untreated p62 is stained in green and nuclei were labeled by DAPI (blue). Cells displaying ≥ 10 γ -H2AX foci were counted as positive. (Data represents 2 independent experiments; $n=4$, mean \pm SEM; P by 2-tailed t test.). **b**, Flow cytometry of BrdU incorporation by WT and Beclin 1- deficient ICAM2⁺ macrophages. (2 independent experiments; *Becn1^{ff}*, $n=6$ vs. *Becn1^{mve\Delta}*, $n=8$; mean \pm SEM; not significant by 2-tailed t test.). **c**, WT and Beclin 1-deficient ICAM2⁺ macrophages were enumerated after IL-4c injections (3 independent experiments; *Becn1^{ff}*+PBS, $n=11$; *Becn1^{mve\Delta}*+PBS, $n=16$; *Becn1^{ff}*+IL4c, $n=11$; *Becn1^{mve\Delta}*+IL4c, $n=19$), and analyzed for frequency of BrdU⁺ and RELM α level (2 independent experiments; *Becn1^{ff}*+PBS, $n=6$; *Becn1^{mve\Delta}*+PBS, $n=9$; *Becn1^{ff}*+IL4c, $n=11$; *Becn1^{mve\Delta}* + IL4c, $n=11$; mean \pm SEM; P_{adj} by Tukey's multiple comparisons test.).

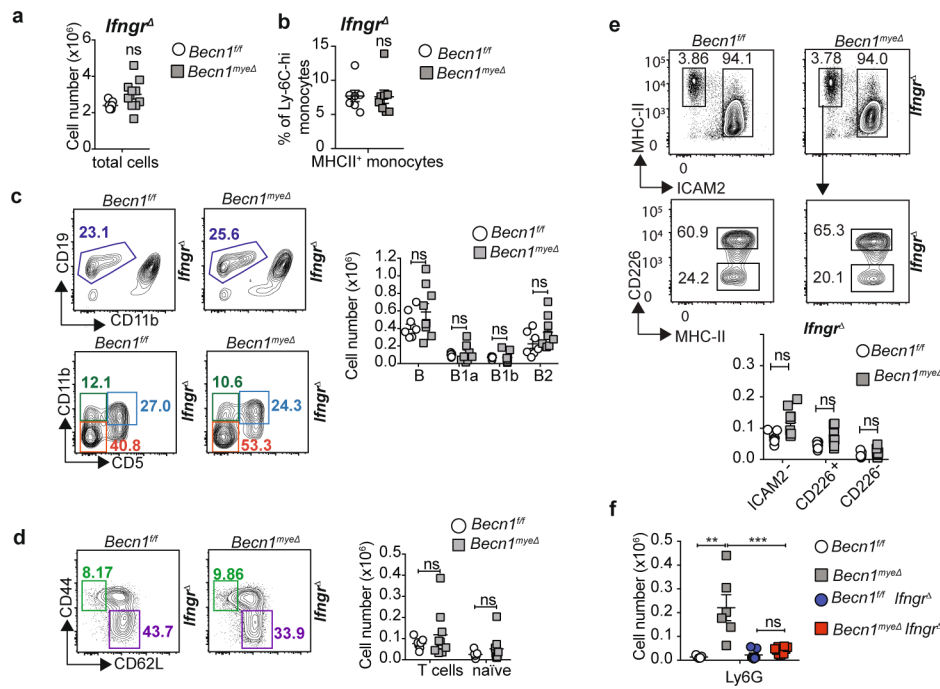


Extended Data Fig. 6 | Peritoneal lymphocytes changes revealed by Single-cell RNA sequencing. **a** and **c**, Violin plots showing the expression of marker genes of B (**a**) and T (**c**) cells clusters by single cell RNAseq. Bar graph comparing fraction size of clusters. **b** and **d**, Flow cytometry validation on naïve mice (*Becn1^{ff}*, $n=9$; *Becn1^{mveΔ}*, $n=10$; mean \pm SEM; P and P_{adj} for multiple comparison, by 2-tailed t test). **e**, *Ifng* transcript level among clusters revealed by single cell RNAseq.

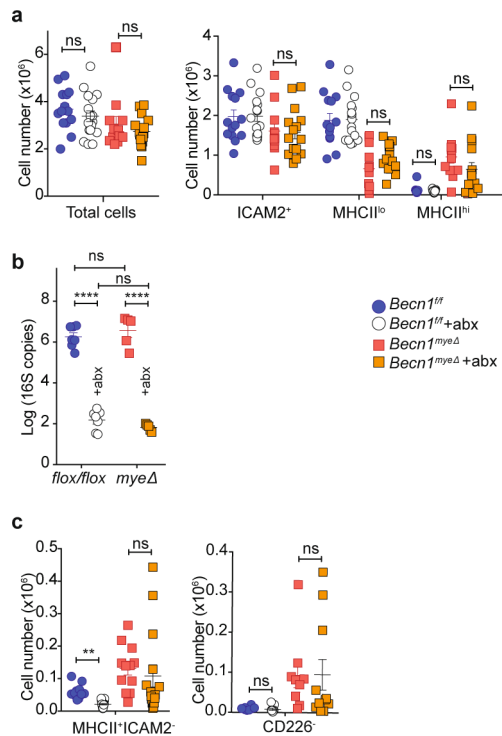


Extended Data Fig. 7 | Peritoneal macrophage activation in *Becn1^{mycΔ}* mice is independent of inflammasome and adaptive immune response.

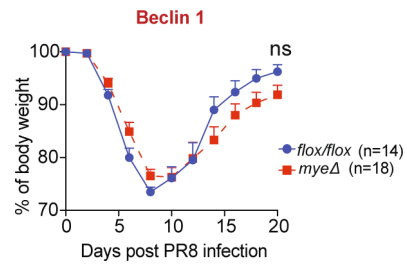
a and **b**, Peritoneal macrophages obtained from naïve mice were analyzed for total cells (**a**), total ICAM2⁺ macrophages, MHC-II^{high} and MHC-II^{low} fractions of ICAM2⁺ macrophages (**b**) by flow cytometry (*Becn1^{fl}/Casp1/11^Δ*, n=6; *Becn1^{mycΔ}/Casp1/11^Δ*, n=6; *Becn1^{fl}/Rag1^Δ*, n=7; *Becn1^{mycΔ}/Rag1^Δ*, n=8 mice, mean \pm SEM, P and P_{adj} by unpaired 2-tailed t test). **c** and **d**, Survival of mice after i.p. inoculation of 5x10⁵ CFUs (**c**) or 5x10⁴ CFU (**d**) of *L. monocytogenes* (Data pooled from 3-4 experiments, P by Log-rank Mantel-Cox test).



Extended Data Fig. 8 | Ifngr^Δ rescues peritoneal immune cell homeostasis in Beclin1^{myeΔ} mice. **a–e**, Flow cytometry analysis of total cells (**a**), B cells (**b**), T cells (**c**), SPM and monocytes (**d**), and peritoneal neutrophils (**e**) and obtained from naïve mice of the indicated genotypes. (Data are from 2 independent experiments; Beclin1^{ff}, $n=8$ vs. Beclin1^{myeΔ}, $n=9$; mean \pm SEM; not significant by 2-tailed Mann-Whitney test.). **f**, Blood neutrophils were analyzed by flow cytometry. ($n=6$; mean \pm SEM; P by 2-tailed Mann-Whitney test.).



Extended Data Fig. 9 | Peritoneal macrophage activation in *Beclin1^{myeΔ}* mice is independent of the presence of microbiota. **a** and **c**, Quantification of total peritoneal cells and ICAM2⁺ macrophages (**a**) and numbers of ICAM2⁺ macrophages and CD226⁺ fraction of ICAM2⁺ macrophages (**c**) (P_{adj} by Dunn's multiple comparisons test). *Beclin1^{+/+}*(Kool-Aid), $n=7$; *Beclin1^{+/+}*(abx), $n=9$; *Beclin1^{myeΔ}*(Kool-Aid), $n=9$; *Beclin1^{myeΔ}*(abx), $n=10$; mean \pm SEM, P_{adj} by one-way ANOVA with Dunn's multiple comparisons test). **b**, Quantification of 16S copy number from stool samples of mice. (*Beclin1^{+/+}*, $n=7$ each for kool-aid and abx vs. *Beclin1^{myeΔ}*, $n=5$ each for kool-aid and abx; mean \pm SEM, P_{adj} analyzed by Tukey's multiple comparisons test).



Extended Data Fig. 10 | *Beclin 1^{myeΔ}* mice did not exhibit enhanced resistance to pulmonary influenza infection. Mice were infected intranasally with 250 TCID₅₀ influenza A PR8 and monitored for weight loss. (Data pooled from 4 independent experiments, mean \pm SEM, not significant by 2way ANOVO for the whole curve or by 2-tailed t test for each time point).

Corresponding author(s): Yating Wang

Last updated by author(s): 10/25/2019

Reporting Summary

Nature Research wishes to improve the reproducibility of the work that we publish. This form provides structure for consistency and transparency in reporting. For further information on Nature Research policies, see [Authors & Referees](#) and the [Editorial Policy Checklist](#).

Statistics

For all statistical analyses, confirm that the following items are present in the figure legend, table legend, main text, or Methods section.

n/a Confirmed

- The exact sample size (n) for each experimental group/condition, given as a discrete number and unit of measurement
- A statement on whether measurements were taken from distinct samples or whether the same sample was measured repeatedly
- The statistical test(s) used AND whether they are one- or two-sided
Only common tests should be described solely by name; describe more complex techniques in the Methods section.
- A description of all covariates tested
- A description of any assumptions or corrections, such as tests of normality and adjustment for multiple comparisons
- A full description of the statistical parameters including central tendency (e.g. means) or other basic estimates (e.g. regression coefficient) AND variation (e.g. standard deviation) or associated estimates of uncertainty (e.g. confidence intervals)
- For null hypothesis testing, the test statistic (e.g. F , t , r) with confidence intervals, effect sizes, degrees of freedom and P value noted
Give P values as exact values whenever suitable.
- For Bayesian analysis, information on the choice of priors and Markov chain Monte Carlo settings
- For hierarchical and complex designs, identification of the appropriate level for tests and full reporting of outcomes
- Estimates of effect sizes (e.g. Cohen's d , Pearson's r), indicating how they were calculated

Our web collection on [statistics for biologists](#) contains articles on many of the points above.

Software and code

Policy information about [availability of computer code](#)

Data collection

BD FACSDiva For scRNASeq, The Cell Ranger Single-Cell Software Suite (version 2.0.2) (<https://support.10xgenomics.com/single-cell-gene-expression/software/pipelines/latest/what-is-cell-ranger>) was used to perform sample demultiplexing, barcode processing, and single-cell 3' counting.

Data analysis

Flowjo and Prism 7 software. Heatmap were generated using Phantasm web service (<https://artyomovlab.wustl.edu/phantasm/>). For the analysis of scRNASeq data, the Seurat package (version 2.3.4) was used.

For manuscripts utilizing custom algorithms or software that are central to the research but not yet described in published literature, software must be made available to editors/reviewers. We strongly encourage code deposition in a community repository (e.g. GitHub). See the Nature Research [guidelines for submitting code & software](#) for further information.

Data

Policy information about [availability of data](#)

All manuscripts must include a [data availability statement](#). This statement should provide the following information, where applicable:

- Accession codes, unique identifiers, or web links for publicly available datasets
- A list of figures that have associated raw data
- A description of any restrictions on data availability

All other data are available from the corresponding authors on reasonable request.

Field-specific reporting

Please select the one below that is the best fit for your research. If you are not sure, read the appropriate sections before making your selection.

Life sciences Behavioural & social sciences Ecological, evolutionary & environmental sciences

For a reference copy of the document with all sections, see nature.com/documents/nr-reporting-summary-flat.pdf

Life sciences study design

All studies must disclose on these points even when the disclosure is negative.

| | |
|-----------------|--|
| Sample size | Sample size is mentioned for each experiment. For western blot analyses and autophagy analyses, three mice per genotype were used for each analysis. This sample size is sufficient to determine whether there is a biologically meaningful difference between different genotypes. For Listeria susceptibility analysis, the maximum number of wild-type and mutant littermates born within a week period were used for each experiment and the experiments were repeated 3-4 times. For flow cytometric analyses of immune cells, ≥3 age-matched littermates of WT and mutant mice were sacrificed for each experiment and the experiments were repeated ≥2 times. No statistical methods were used to predetermine sample size. |
| Data exclusions | no data were excluded |
| Replication | All attempts at replication were successful. |
| Randomization | Groups were established based off of genotype and infection status. Experimental groups consisted of littermates of different genotypes. All other aspects were randomized. |
| Blinding | All data acquisition and analysis was performed by investigators blinded to experimental group. |

Reporting for specific materials, systems and methods

We require information from authors about some types of materials, experimental systems and methods used in many studies. Here, indicate whether each material, system or method listed is relevant to your study. If you are not sure if a list item applies to your research, read the appropriate section before selecting a response.

Materials & experimental systems

| | |
|-------------------------------------|---|
| n/a | Involved in the study |
| <input type="checkbox"/> | <input checked="" type="checkbox"/> Antibodies |
| <input checked="" type="checkbox"/> | <input type="checkbox"/> Eukaryotic cell lines |
| <input checked="" type="checkbox"/> | <input type="checkbox"/> Palaeontology |
| <input type="checkbox"/> | <input checked="" type="checkbox"/> Animals and other organisms |
| <input checked="" type="checkbox"/> | <input type="checkbox"/> Human research participants |
| <input type="checkbox"/> | <input type="checkbox"/> Clinical data |

Methods

| | |
|-------------------------------------|--|
| n/a | Involved in the study |
| <input checked="" type="checkbox"/> | <input type="checkbox"/> ChIP-seq |
| <input type="checkbox"/> | <input checked="" type="checkbox"/> Flow cytometry |
| <input checked="" type="checkbox"/> | <input type="checkbox"/> MRI-based neuroimaging |

Antibodies

Antibodies used

For flowcytometry: anti-FcγRII/III (biologen 101302) and labeled with specific antibodies against CSF1R (eBioscience 46-1152-80), ICAM2 (Biologen 105606), F4/80 (eBioscience 25-4801-82), CD226 (biologen 128805), Ly-6G (BioLegend 127624), I-A/I-E (BioLegend 107631), CD11b (BioLegend 101237), TCRb (eBioscience 11-5961-85), CD19 (BD 552854), CD5 (BD 553022), CD62L (BioLegend 104432), CD44 (BioLegend 103012).

Validation

All antibodies validation are available on the manufacturers' websites.

Animals and other organisms

Policy information about [studies involving animals](#); [ARRIVE guidelines](#) recommended for reporting animal research

Laboratory animals

Atg5f/f and Atg5f/f-Lyz2cre+/- mice were generated as described previously in an enhanced barrier facility. Becn1f/f-Lyz2cre+/-, Fip200f/f-Lyz2cre+/-, Atg7f/f-Lyz2cre+/-, and Atg16l1f/f-Lyz2cre+/- were generated in the same way as Atg5f/f-Lyz2cre+/-, Becn1f/f-CD11c-cre+/-, and Becn1f/f-Mrp8-cre+/- were generated by breeding Becn1f/f to CD11ccre+/- (#007567) and Mrp8-cre+/- (#021614) from the Jackson Laboratory. Rubicon-/- knockout mice were kindly provided by Doug Green and Jennifer Martinez. Rag1-/- (#002216), Ifngr-/- (#003288), and Casp1/11-/- (#016621) mice were from the Jackson

Laboratory. All mice used for experimental procedures were 8–12 weeks of age and sex matched littermates unless specified otherwise.

Wild animals

Provide details on animals observed in or captured in the field; report species, sex and age where possible. Describe how animals were caught and transported and what happened to captive animals after the study (if killed, explain why and describe method; if released, say where and when) OR state that the study did not involve wild animals.

Field-collected samples

For laboratory work with field-collected samples, describe all relevant parameters such as housing, maintenance, temperature, photoperiod and end-of-experiment protocol OR state that the study did not involve samples collected from the field.

Ethics oversight

Mice were housed and bred at Washington University in St. Louis in specific pathogen-free conditions in accordance with federal and university guidelines, and protocols were approved by the Animal Studies Committee of Washington University.

Note that full information on the approval of the study protocol must also be provided in the manuscript.

Flow Cytometry

Plots

Confirm that:

- The axis labels state the marker and fluorochrome used (e.g. CD4-FITC).
- The axis scales are clearly visible. Include numbers along axes only for bottom left plot of group (a 'group' is an analysis of identical markers).
- All plots are contour plots with outliers or pseudocolor plots.
- A numerical value for number of cells or percentage (with statistics) is provided.

Methodology

Sample preparation

sample preparation is listed in Methods

Instrument

LSRFortessa (BD Biosciences)

Software

FACSDiva for collection and FlowJo for analysis

Cell population abundance

Populations were validated for purity by a post-sort analysis by FACS

Gating strategy

Every flow cytometry analysis was initiated as follows:
FSC-A/H and SSC-A/H to gate the singlet population and then as described in supplemental figures.

Tick this box to confirm that a figure exemplifying the gating strategy is provided in the Supplementary Information.